Available online at www.sciencedirect.com
SCIENCE DIRECT®
International Journal of Solids and Structures 43 (2006) 4997–5031
INTERNATIONAL JOURNAL OF SOLIDS and STRUCTURES
www.elsevier.com/locate/ijsolstr

Wave propagation analysis in anisotropic and inhomogeneous uncracked and cracked structures using pseudospectral finite element method

R. Sridhar, A. Chakraborty, S. Gopalakrishnan *

Department of Aerospace Engineering, Indian Institute of Science, Bangalore 560012, India

Received 14 April 2005; received in revised form 31 August 2005
Available online 15 December 2005

Abstract

The work deals with the development of an effective numerical tool in the form of pseudospectral method for wave propagation analysis in anisotropic and inhomogeneous structures. Chebyshev polynomials are used as basis functions and Chebyshev–Gauss–Lobatto points are used as grid points. The formulation is implemented in the same way as conventional finite element method. The element is tested successfully on a variety of problems involving isotropic, orthotropic and functionally graded material (FGM) structures. The formulation is validated by performing static, free vibration and wave propagation analysis. The accuracy of the element in predicting stresses is compared with conventional finite elements. Free vibration analysis is carried out on composite and FGM beams and the computational resources saved in each case are presented. Wave propagation analysis is carried out using the element on anisotropic and inhomogeneous beams and layer structures. Wave propagation in thin double bounded media over long propagating distances is studied. Finally, a study on scattering of waves due to embedded horizontal and vertical cracks is carried out, where the effectiveness of modulated pulse in detecting small cracks in composites and FGMs has been demonstrated.

Keywords: Chebyshev polynomial; FGM; Composite; High frequency; Structural health monitoring; Wave scattering

1. Introduction

Over the years, many analytical techniques have been developed for treating wave propagation problems. Central among these is the method of Fourier synthesis or the spectral analysis (Doyle, 1997), where the behavior of the signal is viewed as a superposition of many infinitely long wave trains of different periods (or frequencies). The actual response is synthesized by a judicious combination of these wave trains. Thus the problem of characterizing a signal is transformed into one of determining the set of combination

* Corresponding author. Fax: +91 80 2360 0134.
E-mail address: krishnan@aero.iisc.ernet.in (S. Gopalakrishnan).

0020-7683/$ - see front matter © 2005 Elsevier Ltd. All rights reserved.
doi:10.1016/j.ijsolstr.2005.10.005

coefficients. These coefficients are called the Fourier transform of the signal. While the problem being tackled invariably simplifies when it is expressed in terms of the Fourier transform, the last step in the analysis involves performing an inverse transform (reconstruction the signal) and this, generally, is very difficult to do in an exact analytical manner. Consequently, many approximate and asymptotic schemes have usually been resorted to.

Realistic numerical simulation of wave propagation phenomena requires huge computational resource. High-order techniques have attracted high interest in the last years, as means to improve computational efficiency and reduce computation time needed for a simulation. They have been introduced within several methodological frameworks, such as finite difference, finite element, and pseudospectral methods. Independent of the approach, the approximated solution is described in terms of high-order polynomial basis. High-order techniques are always associated with not only high accuracy and computational efficiency but also some well-known drawbacks. For instance, finite difference methods are not very well suited for describing very complex geometries and heterogeneous media, boundary conditions are difficult to implement. Last but not the least, classical high-order finite elements (FEs) are known to generate high-order spurious modes.

To overcome these problems, the spectral element method has been developed. It combines the accuracy of spectral methods with the flexibility of the FEs. So called "spectral-element" methods gain the best of both worlds by hybridizing spectral and finite element methods. The domain is subdivided into elements, as in FEs, to gain the flexibility and matrix sparsity of FEs. At the same time, the degree of the polynomial in each sub-domain is sufficiently high to retain the high accuracy and low storage of spectral methods. However, the spectral methods also have their own set of drawbacks.

The drawbacks of spectral methods are threefold. First, they are usually more difficult to program than finite difference procedures. Second, they are more costly per degree of freedom than finite difference procedures. Third, irregular domains inflict heavier losses of accuracy and efficiency on spectral algorithms than on lower order alternatives. However, over the past twenty years the above drawbacks have been minimized by proper implementation of the "pseudospectral methods".

The spectral approach is based on choosing proper basis functions, similar to the sine and cosine terms of a Fourier series, which lead to a high rate of convergence of a series that represents the solution. The pseudospectral methods associate a grid of points $\{x_i\}$ called the "grid points" or "collocation points" with each basis set (or function). The coefficients $\{a_n\}$ of a pseudospectral approximation to the solution of a differential equation are found by requiring that the residual function interpolated (difference between exact and approximate functions) is zero at the grid points, i.e.,

$$R(x_i; a_0, a_1, \ldots, a_N) = 0, \quad i = 0, 1, \ldots, N.$$

In other words, the pseudospectral method demands that the governing differential equation be exactly satisfied at a set of points known as the "collocation" or "interpolation" points. Presumably, as the residue $R(x; a_n)$ is forced to vanish at an increasingly large number of discrete points, there will be smaller and smaller gaps between the collocation points so that $R \approx 0$ everywhere in the domain. Pseudospectral methods are also called "orthogonal collocation" or "method of selected points".

As N is increased, the pseudospectral methods benefit in two ways. First the interval h between two adjacent grid points becomes smaller. This would cause the error to rapidly decrease even if the order of the method were fixed. Unlike finite difference or finite element methods, however, the order in not fixed. When N increases from 10 to 20, the error becomes $O(h^{20})$ in terms of the new, smaller h. Since h is $O(1/N)$, we have,

$$\text{Pseudospectral error} \approx O[(1/N)^N].$$

Thus, the error is decreasing faster than any finite power of N because the power in the error formula is always increasing too. This is called the "*infinite order*" or "*exponential*" convergence.

Pseudospectral methods can yield good results even when many decimal places of accuracy is needed, with about half as many degrees of freedom, as compared to a lower order methods. In other words, pseudospectral methods, because of their high accuracy, are *memory minimizing*. Problems that require high resolution can often be done satisfactorily by pseudospectral methods when a three-dimensional second-order finite difference code would fail because of the need for eight or ten times as many grid points which would exceed the core memory of the available computer.

The pseudospectral method can be considered to be a spectral method that performs a collocation process. Pseudospectral analysis consists of selection of basis functions and the collocation points. Fourier series, Chebyshev polynomials, Legendre polynomials etc., are the commonly used basis functions. The choice of basis function is primarily guided by the type of problem (whether periodic or non-periodic) and the geometry. In the present work, pseudospectral method based on Chebyshev polynomials, which are ideal for non-periodic problems, is used. Chebyshev polynomials are well established in interpolation theory as being min–max interpolants and Gottlieb and Orzag (1977) and Boyd (2000) have shown that they possess accuracy and computational economy while solving scalar wave equation. The collocation points used in this work are Chebyshev–Gauss–Lobatto points, which are the most commonly used quadrature points for numerical integration schemes based on Chebyshev polynomials.

The use of Chebyshev spectral FEs to wave propagation problems has been found in a few articles published over the years. Dauksher and Emery (1997) have described the application of Chebyshev spectral element to one-dimensional and two-dimensional scalar wave equations that characterize acoustic waves. They showed that by using high-order Chebyshev spectral elements, it is possible to reduce dispersive effects to the point that the solutions are of very high accuracy. They (Dauksher and Emery, 2000) have applied the same to the solutions of elastostatic and elastodynamic problems in two dimensions. It was shown that the spectral approach can achieve nearly zero dispersion for a wide range of spatial and temporal discretization. The same authors (Dauksher and Emery, 1999) have examined the computational cost associated with finite element solutions to the two-dimensional scalar wave equation with Chebyshev and equispaced Lagrange interpolant based elements. The *p*-type refinement with the Chebyshev spectral elements was shown to be significantly more cost-effective and numerically stable when compared with that of Lagrange elements.

Padovani et al. (1994) compared standard FEM and spectral elements for wave propagation in elastic media. Seriani and Priolo (1994) used the spectral element method for acoustic wave simulation in heterogeneous media. They found that the spectral element method based on Chebyshev polynomials showed more accurate results compared to low-order finite element and the conventional finite difference methods. High accuracy was reached even for rather long wave propagation and dispersion errors were essentially eliminated. Further, Priolo et al. (1994) presented Chebyshev spectral element and pseudospectral method for wave simulation at the interface of different elastic media. Recently, Seriani (2004) developed the double-grid Chebyshev spectral elements for acoustic wave modeling and carried out wave propagation analysis in inhomogeneous media.

Patera (1984) developed finite element shape functions based on the Chebyshev series for the solution of laminar flow problems. Jackiewicz and Renaut (2002) dealt with the effects on stability, of subtle differences in formulations of pseudospectral methods for solution of the acoustic wave equation. Soni and Amba-Rao (1975) and Gupta and Lal (1985) are among those who applied the pseudospectral method to the axisymmetric vibration analysis of circular and annular Mindlin plates. Recently the usefulness of the pseudospectral method in the solution of structural mechanics problems has been demonstrated in a static analysis of the L-shaped Reissner–Mindlin plate by Lee (1998). Lee and Schultz (2004) studied the free vibration of Timoshenko beams and axisymmetric Mindlin plates using the Chebyshev pseudospectral method.

The available literature suggests that the use of pseudospectral element methods has been quite limited in the fields of structural mechanics, structural dynamics and wave propagation. As the formulation is straight forward and powerful enough to produce approximate solutions close to exact solutions, this method has been highly successful in many areas such as turbulence modeling, weather prediction and non-linear waves. Even though this method can be used for the solution of structural mechanics problems, it has been largely unnoticed by the structural mechanics community, and few articles are available where the pseudospectral method has been applied.

Thus, the present work is aimed at developing a numerical tool in the form of pseudospectral finite element method that has the advantages of conventional finite element method and a low computational cost on account of its spectral convergence. An attempt is made to develop pseudospectral finite element method based on Chebyshev polynomials as an efficient numerical tool for handling wave propagation problems. It shall henceforth be referred to as Chebyshev pseudospectral element method (CPEM). CPEM thus developed is mainly intended to solve wave propagation problems involving anisotropic materials like composites and inhomogeneous materials like the functionally graded materials (FGM). This is further been extended to structural health monitoring applications, wherein the wave scattering due to the presence of vertical and

horizontal cracks in both anisotropic and inhomogeneous structures is studied. Also, these models are used to detect the presence of cracks using a tone-burst modulated pulse.

The organization of the paper is as follows. In the next section, the details of the element formulation is given, where attention is given to both anisotropic and inhomogeneous material. Subsequently, the static, free vibration and wave propagation analyses have been performed in Sections 3–5, respectively. Section 6 gives the details of crack modeling and wave scattering studies and conclusions are drawn in Section 7.

2. Development of Chebyshev pseudospectral element

The equations of dynamic equilibrium for a two-dimensional region in rectangular Cartesian coordinate system are

$$\frac{\partial \sigma_{xx}}{\partial x}+\frac{\partial \sigma_{xy}}{\partial y}=\rho\frac{\partial^2 u}{\partial t^2}, \qquad \frac{\partial \sigma_{xy}}{\partial x}+\frac{\partial \sigma_{yy}}{\partial y}=\rho\frac{\partial^2 v}{\partial t^2}, \tag{1}$$

where u and v are the components of the displacements field in x- and y-directions, respectively and ρ is the material density.

The finite element method (FEM) or CPEM approach requires the computational domain to be decomposed into triangular or rectangular sub-domains. Then, the solution is expressed in terms of the interpolation functions or the "*shape functions*". This leads to the approximation of the equilibrium equations (Eq. (1)) in the following form:

$$M^{\mathrm{g}}\frac{\mathrm{d}^2 u}{\mathrm{d}t^2}+K^{\mathrm{g}}u=f^{\mathrm{g}}, \tag{2}$$

where the global mass and stiffness matrices, designated as M^{g} and K^{g}, result from the sum of element contributions of each node. The f^{g} is a column vector of applied forces.

It may be seen that Eq. (2) is a linear, second-order, ordinary differential equation, which must be integrated in time to obtain the variation of the displacement field over time. Among the available schemes, time integration is performed using an implicit Newmark scheme (Cook et al., 1989), which guarantees unconditional stability.

In terms of the shape functions, Ψ_I, the element contributions at a node result from the integrals over the element area $\widehat{\Omega}_{\mathrm{e}}$

$$M_{IJ}=\int_{\hat{\Omega}_{\mathrm{e}}}\rho\Psi_I\Psi_J t\,\mathrm{d}x\,\mathrm{d}y, \tag{3}$$

$$K_{IJ}=\int_{\hat{\Omega}_{\mathrm{e}}}B_I^T D B_J t\,\mathrm{d}x\,\mathrm{d}y, \tag{4}$$

where t is the thickness of the material. The I and J both range over the all the degrees of freedom (dof) at each node in the element. The D is the constitutive relation matrix, which is constant for anisotropic material and spatially dependent for FGM. The strain displacement matrix B_I is defined as

$$B_I=\begin{bmatrix}\dfrac{\partial\Psi_I}{\partial x} & 0\\ 0 & \dfrac{\partial\Psi_I}{\partial y}\\ \dfrac{\partial\Psi_I}{\partial y} & \dfrac{\partial\Psi_I}{\partial x}\end{bmatrix}.$$

The integrals in Eqs. (3) and (4) can be evaluated by a quadrature rule in the natural coordinate system. Legendre–Gauss quadrature is used in the present case.

Patera (1984) developed the finite element shape functions based on the Chebyshev polynomials for the solution of laminar flow problems. These shape functions are defined in the natural coordinates system $\widehat{\Omega}=[-1\leqslant\xi\leqslant 1]\times[-1\leqslant\eta\leqslant 1]$ as

$$\Psi_I = \Psi_i(\xi)\Psi_j(\eta) = \left\{ \frac{2}{N_\xi} \sum_{n=0}^{N_\xi} \frac{1}{c_i c_n} T_n(\xi_i) T_n(\xi) \right\} \left\{ \frac{2}{N_\eta} \sum_{m=0}^{N_\eta} \frac{1}{c_j c_m} T_m(\eta_j) T_m(\eta) \right\}, \tag{5}$$

where $1 \leqslant I \leqslant (N_\xi + 1)(N_\eta + 1)$, $0 \leqslant i \leqslant N_\xi$ and $0 \leqslant j \leqslant N_\eta$. There are $N_\xi + 1$ nodes in ξ direction and $N_\eta + 1$ nodes in η direction. The constants $c_j = 1$ for $0 < j < N$ and 2 for $j = 0$, N. T_j are the Chebyshev polynomials of the first kind and are given by,

$$T_j(\cos\theta) = \cos(j\theta). \tag{6}$$

Using the mapping $x = \cos\theta$, the Chebyshev polynomials in Eq. (6) can be written as,

$$T_j(x) = \cos(j\cos^{-1}x). \tag{7}$$

Thus, Chebyshev polynomials are nothing but cosine functions after a change in the independent variable. This property is the origin of their widespread popularity in the numerical approximation of non-periodic boundary value problems. The transformation $x = \cos\theta$ enables many mathematical relations as well as theoretical results concerning the Fourier system to be adapted readily to the Chebyshev system. The Chebyshev polynomials satisfy the following recurrence relation:

$$T_{k+1}(x) = 2xT_k(x) - T_{k-1}(x), \tag{8}$$

with $T_0(x) \equiv 1$ and $T_1(x) \equiv x$.

The grid points to be used for CPEM are the quadrature points corresponding to Chebyshev polynomials. The most commonly used points are those for Gauss–Lobatto case, which are

$$x_i = -\cos\frac{\pi i}{N}, \quad \text{where } i = 0, 1, \ldots, N. \tag{9}$$

The shape function $\Psi_i(\xi)$ is plotted in Fig. 1 for $N_\xi = 1$, 2, 3 and 4. $N_\xi = 1$ produces the linear algebraic shape functions and $N_\xi = 2$ produces the quadratic shape functions, which are the same as those for equispaced Lagrangian FEs. As illustrated, for the higher order elements ($N > 2$), the spectral element is different from the conventional FEs.

As already mentioned, the position of the grid points are the quadrature points for Chebyshev–Gauss–Lobatto case, and are given by Eq. (9). The placement of nodes in the natural coordinate system follows the trigonometric relationships:

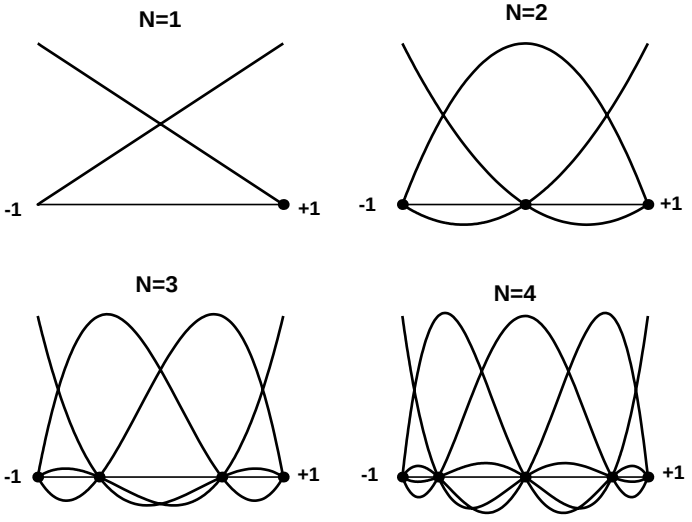

Fig. 1. Chebyshev shape functions for $N = 1$, 2, 3 and 4.

$$\xi_i = -\cos\frac{\pi i}{N_\xi} \quad \text{where } i = 0, 1, \ldots, N_\xi,$$

$$\eta_j = -\cos\frac{\pi j}{N_\eta} \quad \text{where } j = 0, 1, \ldots, N_\eta.$$

The position of the nodes (or grid points) for the Chebyshev pseudospectral elements of different orders and the corresponding equispaced Lagrange elements are shown in Fig. 2.

As can be seen from Fig. 2, the CPE and the equispaced Lagrange finite element are essentially same for $N = 1$ and $N = 2$. However for values of $N > 2$, the nodes are located closer to the corners of the element unlike the conventional finite element where the nodes are located at equal spacing. Therefore, hereafter $N = 1$ and $N = 2$ shall be referred to as FEs and $N \geqslant 3$ as Chebyshev pseudospectral elements (CPE).

The equations for evaluating the mass and stiffness matrix of each element in the domain is given by Eqs. (3) and (4), respectively. The element integrals are in the global domain while the shape functions are in the element's natural coordinate system. This integration is done using Jacobian mapping and Gauss–Legendre integration (Canuto et al., 1988). The above integrations get transformed as follows in the natural coordinate system of each element:

$$M_{IJ} = \int_{-1}^{1}\int_{-1}^{1} \rho \Psi_I \Psi_J |J| t \, \mathrm{d}\xi \, \mathrm{d}\eta, \tag{10}$$

$$K_{IJ} = \int_{-1}^{1}\int_{-1}^{1} B_I^T D B_J |J| t \, \mathrm{d}\xi \, \mathrm{d}\eta, \tag{11}$$

where $|J|$ denotes the determinant of the Jacobian matrix of the coordinate transformation. It is to be noted that the coordinates of all the nodes are not essential to generate the Jacobian matrix, which is evaluated using the coordinates of the four corner nodes only. In other words, geometry is always being mapped by $N = 1$ Chebyshev shape functions. Hence, *sub-parametric mapping* is carried out (except when $N = 1$) where-in the geometry is mapped by a polynomial of lower order as compared to the one used for mapping the field variables.

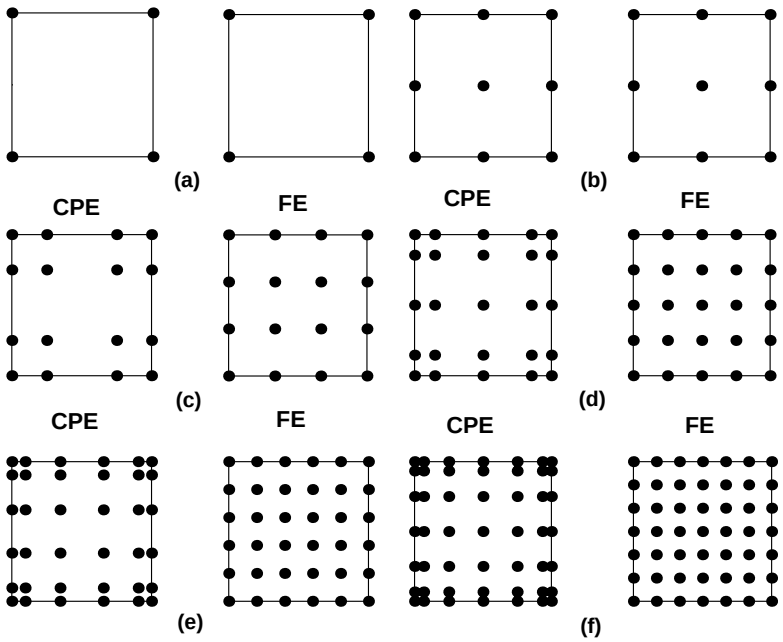

Fig. 2. Placement of nodes for Chebyshev pseudospectral element (CPE) and finite element (FE) for (a) $N_\xi = N_\eta = 1$, (b) $N_\xi = N_\eta = 2$, (c) $N_\xi = N_\eta = 3$, (d) $N_\xi = N_\eta = 4$, (e) $N_\xi = N_\eta = 5$, (f) $N_\xi = N_\eta = 6$.

2.1. Constitutive relation: anisotropic and inhomogeneous material

The matrix D establishes the relation between the stress and strain in the anisotropic and inhomogeneous material. For anisotropic materials, its elements are dictated by the three Young's moduli (E_1, E_2 and E_3 in the three principal material direction), three shear moduli (G_{23}, G_{13} and G_{12}) and three Poisson's ratio (ν_{23}, ν_{13} and ν_{12}). The relation between the elements of the D matrix (6×6) and these parameters can be found in Reddy (1997). For 2-D analysis, the D matrix needs to be reduced into a 3×3 matrix by plane-stress, plane-strain or axi-symmetric reduction as may be the case.

In the case of inhomogeneous material like FGM, the density and elastic properties vary from point to point on it. They can be both isotropic and anisotropic in nature, however, the FGM, which is generally made of ceramic and metal is essentially isotropic in nature. Thus, the Young's modulus and Poisson's ratio of the metal or ceramic govern the elements of the D matrix. For, FGM, the density and Young's modulus vary from point to point and the Poisson's ratio is assumed constant.

The variation of the properties in a structure may be in any direction namely lengthwise or depthwise. They are accordingly called lengthwise FGM or depthwise FGM. To incorporate inhomogeneity in the formulation, we introduce two parameters density multiplication factor (β) and Young's modulus multiplication factor (α), which are functions of the coordinates of the point in the material. Multiplying the density and Young's modulus of a homogeneous material by β and α, respectively, gives the values of these properties at corresponding point in the FGM. Generally, the variation of these parameters in FGM is assumed to be according to power law or exponential law (Chakraborty et al., 2003) as illustrated below.

A lengthwise graded FGM bar of length 1 m is considered. It is composed of steel (0.25 m) and ceramic (0.25 m) at the two ends of the beam and in between there is FGM, which smoothly blends the properties of the steel ($E = 200 \times 10^9$ N/m^2, $\rho = 7800$ kg/m^3) to that of ceramic ($E = 390 \times 10^9$ N/m^2, $\rho = 3950$ kg/m^3). The power law or exponential variation of β can be stated as in Eqs. (12) and (13), respectively.

$$\begin{aligned} \beta(x) &= 1; \quad x \leqslant x_1 \\ &= ax^n + b; \quad x_1 \leqslant x \leqslant x_2 \\ &= \frac{\rho_2}{\rho_1}; \quad x_2 \leqslant x \leqslant L, \end{aligned} \tag{12}$$

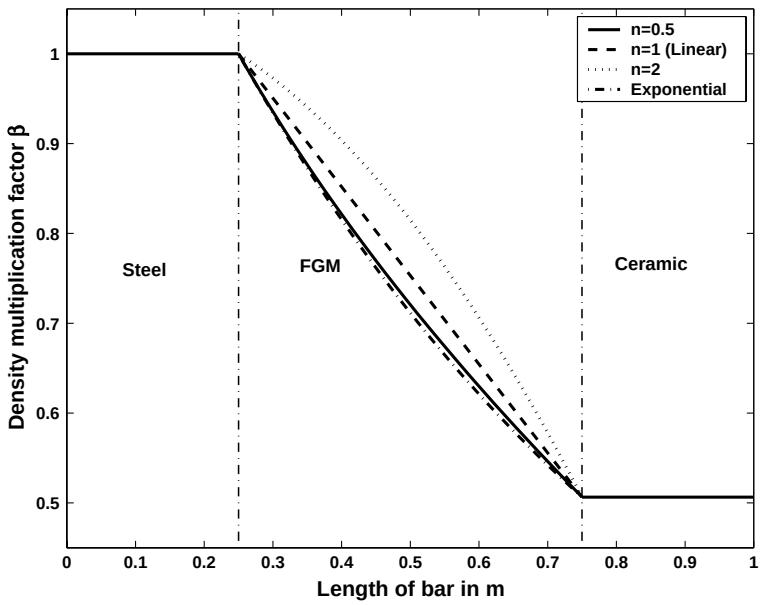

Fig. 3. Variation of density multiplication factor β along the length of FGM bar.

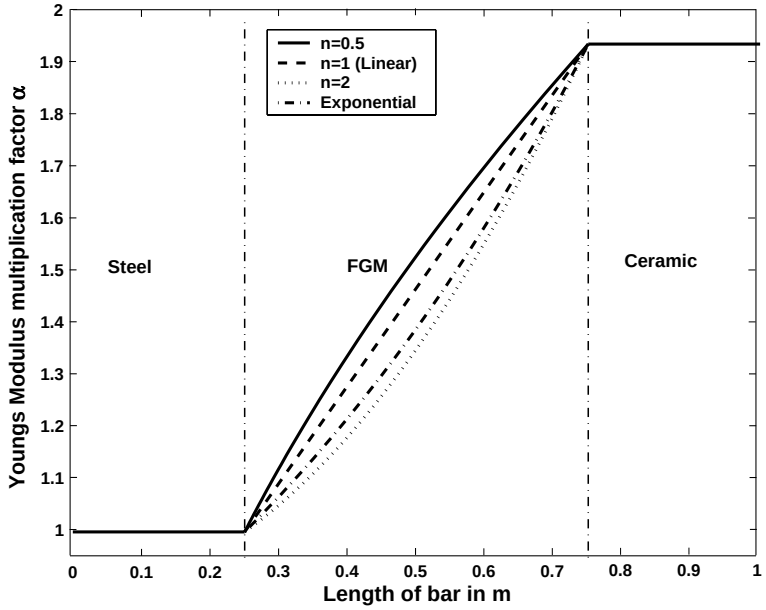

Fig. 4. Variation of Young's modulus multiplication factor α along the length of FGM bar.

$$\begin{aligned}\beta(x) &= 1; \;\; x \leqslant x_1 \\ &= ae^{bx}; \;\; x_1 \leqslant x \leqslant x_2 \\ &= \frac{\rho_2}{\rho_1}; \;\; x_2 \leqslant x \leqslant L. \end{aligned} \tag{13}$$

In the above equations, x_1 and x_2 are the length coordinates of the interface between homogeneous portions and FGM. L is the total length of the rod. ρ_1 and ρ_2 are the denisities of the homogeneous components of the rod. a and b are constants that are determined using the values of β at the interface of the homogenous parts and FGM. Similar equations can be written for variation of α also.

The variation of β and α along the length of the bar for both power and exponential law is shown in Figs. 3 and 4, respectively. As can be seen in Figs. 3 and 4, the values of β and α are constant in the homogeneous part of the bar and follow the variation law in the FGM part.

The density and Young's modulus of each element is obtained by computing them at the corner nodes of the element and interpolating them to the Legendre–Gauss quadrature points (used for numerical integration) using the $N = 1$ (i.e., 2×2) shape functions. The mass and stiffness matrices of the element can then be obtained using these values of density and Young's modulus in Eqs. (10) and (11), respectively.

3. Analysis of static problems

The developed CPE needs to be validated before using it to solve wave propagation problems. In this section, few static problems involving an isotropic material are solved using the CPE.

3.1. Axial case

A steel cantilever beam of 1 m length, 0.1 m thickness and unit width is considered for analysis, which is subjected to a uniformly distributed axial load of 10 N/m at the free end. The material properties of steel are as taken before. The geometry is modeled for analysis using CPE of different orders.

The number of elements required to reach the converged result for $N = 1$, $N = 2$ and $N = 3$ is tabulated in Table I. The table also gives the converged value of the end deflection in each case along with the exact end

Table I
Number of elements, memory required, CPU time taken and computed end deflections for static case with axial load for different values of Chebyshev N

	$N=1$	$N=2$	$N=3$
Number of elements	1	1	1
Memory for stiffness matrix (Bytes)	21	157	601
Total CPU time (s)	0.10	0.10	0.10
Computed end deflection (m)	5×10^{-11}	5×10^{-11}	5×10^{-11}

Exact end deflection $=5\times10^{-11}$ m.

deflection of the bar. The analysis could be carried out using just one element in each case. Table I also gives the memory used for stiffness matrix generation and CPU time taken by the processor. These values are not of much significance in this case.

3.2. Transverse case

Next, the steel beam is subjected to a concentrated load of magnitude $1N$ in the transverse direction at the free end. The number of elements that were required to obtain the converged result along with the memory used, CPU time taken for analysis and computed and exact end deflection for each case is given in Table II. The advantage of using higher value of N is evident from the table. The exact end deflection of the beam is computed using Eq. (14)

$$\delta=\frac{Pl^3}{3EI}+\frac{Pl}{kGA}, \tag{14}$$

where E, G are the Young's modulus and shear modulus of the beam, I, A the moment of inertia about neutral axis and cross-sectional area of the beam. P is the magnitude of the applied concentrated load and l is the span of the beam. The k is the shear correction factor ($k=2/3$).

As already mentioned, the CPE is the same as conventional FE for $N=1$ and 2. For $N\geqslant 3$ the position of the nodes and the shape functions are different for the two. Table II gives us a glimpse of the superiority of CPE. The memory requirement as well as the computational time are considerably reduced from $N=1$ to $N=3$. The computational advantage gained by the use of $N=3$ over $N=1$ and 2 will be even more evident when dynamic analysis is carried out, which will be dealt with in the next two sections.

3.3. Effect of l/d ratio

It may be noted that in the above analysis, the length to depth ratio of the bar was 10 (1 m/0.1 m). The thickness of the beam used in above analysis is now changed to study the effect of l/d ratio on the number of elements required for $N=1$, $N=2$ and $N=3$.

Three cases are considered where the depth of the beam is taken as 0.1 m, 0.01 m and 0.001 m. Thus, the corresponding l/d ratios are 10, 100 and 1000, respectively. The number of elements required for transverse analysis for each case is tabulated in Table III. The values of the computed and exact end deflection for each case is given in Table IV.

Table II
Number of elements, memory required and CPU time taken for static case with transverse load for different values of Chebyshev N

	$N=1$	$N=2$	$N=3$
Number of elements	80	5	1
Memory for stiffness matrix (Bytes)	2881	1201	601
Total CPU time (s)	0.18	0.13	0.10
Computed end deflection (m)	2.00×10^{-8}	2.01×10^{-8}	2.01×10^{-8}

Exact end deflection $=2.015\times10^{-8}$ m.

Table III
Number of elements required for different values of l/d ratio

l/d	10	100	1000
$N=1$	80	4000	15,000
$N=2$	5	30	50
$N=3$	1	1	2

Table IV
Comparison of exact and computed end deflections in metres for different values of l/d ratio

l/d	Exact	$N=1$	$N=2$	$N=3$
10	2.01×10^{-08}	2.00×10^{-08}	2.01×10^{-08}	2.01×10^{-08}
100	2.00×10^{-05}	2.00×10^{-05}	2.00×10^{-05}	2.00×10^{-05}
1000	2.00×10^{-02}	1.99×10^{-02}	2.00×10^{-02}	2.00×10^{-02}

A comparison of the total CPU time and the memory requirement for each analysis is shown in the bar charts given in Fig. 5. The bar diagrams reveal the advantage of using a higher order CPE such as $N=3$ for large l/d ratios. As can be seen, the memory requirement and CPU time are substantially high when $N=1$ and $N=2$ elements are used for l/d ratios of 100 and 1000. This is due to the low rate of convergence of these lower order elements. However, $N=3$ analysis is hardly affected by the increase in the l/d ratio. This is on account of the *spectral convergence* of CPE. Moreover, the deflections predicted by CPE are quite accurate even for high l/d ratios and the element can be said to be free of shear locking.

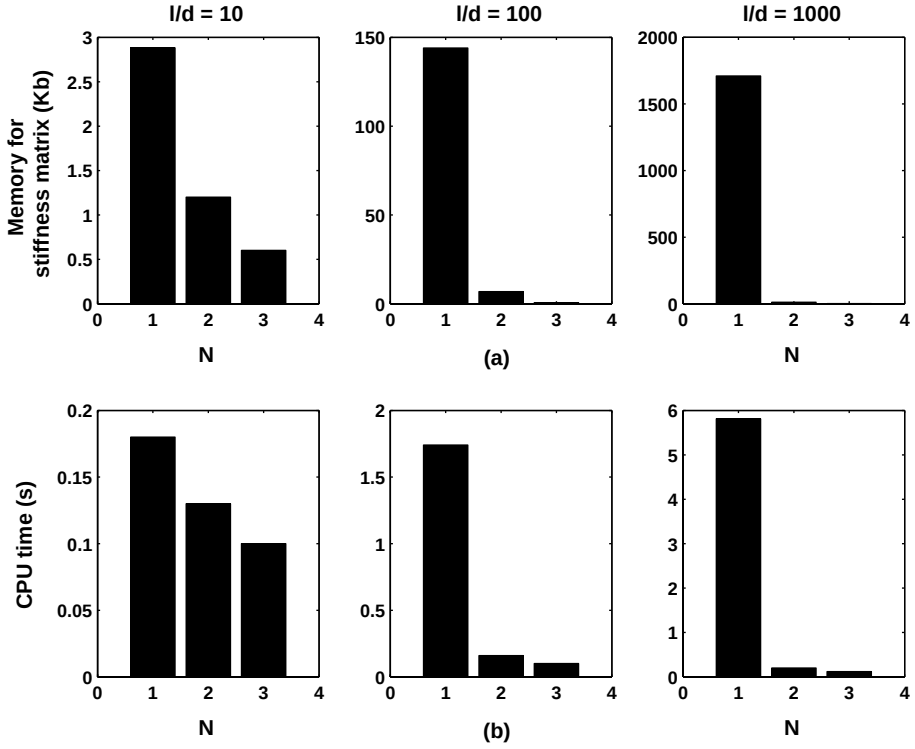

Fig. 5. Comparison of $N=1$, $N=2$ and $N=3$ analysis for different l/d ratios. (a) Memory used for stiffness matrix generation in kilobytes and (b) total CPU time in seconds.

3.4. Stress computation

Using the constitutive matrix (D matrix) and displacements obtained during above analysis (Section 3.2), the stresses (σ_{xx}, σ_{yy} and τ_{xy}) in each element are computed at the Gauss–Legendre quadrature points. Thus, stresses at different locations in the structure are obtained. The stress computation has been done for all the three cases viz., $N = 1$, $N = 2$ and $N = 3$, using the minimum number of elements required for convergence in each case. The contours of the stress (σ_{xx}) obtained for above transverse analysis, for $N = 1$, $N = 2$ and $N = 3$ are plotted in Figs. 6–8, respectively. These are compared with the stress contours plotted using the exact stress values at the corresponding Gauss–Legendre quadrature points.

Fig. 9 gives comparison of the error in stress computation in each case. In all the three cases, stress computation error is minimum near the fixed end of the beam. However, the error in stress values at the free end is about 135% for $N = 1$ and 65% for $N = 2$. On the other hand, the error in the case of $N = 3$ is almost zero throughout.

3.5. Effect of mesh distortion

The CPE ($N = 3$) has been shown to be superior in static analysis for high l/d ratios and also in stress computation. In this section, the effect of mesh distortion on stress prediction is studied.

The beam used in transverse analysis in Section 3.2 is used again. The beam is discretized into 5 elements, all lengthwise. In the first case all the elements are perfect rectangles. Then, analysis is carried out using a completely distorted mesh as shown in Fig. 10. Analysis is carried out using these meshes for all three cases viz., $N = 1$, $N = 2$ and $N = 3$.

The percentage error in prediction of stress (σ_{xx}) at various points in the beam for the undistorted mesh as well as the distorted mesh in each of the analysis is plotted in Fig. 11. As can be seen from the plots, the percentage error in stress computation from the distorted mesh is always higher than that from the undistorted mesh for $N = 1$. For $N = 2$ the mesh distortion results in an increase of error from about 75% to nearly 95% at the free end. However, $N = 3$ analysis is unaffected by mesh distortion. Moreover the magnitude of error is almost negligible at all points. It must be mentioned that for $N = 1$ only one row of elements is used for convenience. This results the large error shown in Fig. 11 for $N = 1$, which can be further reduced by introducing more than one element depthwise.

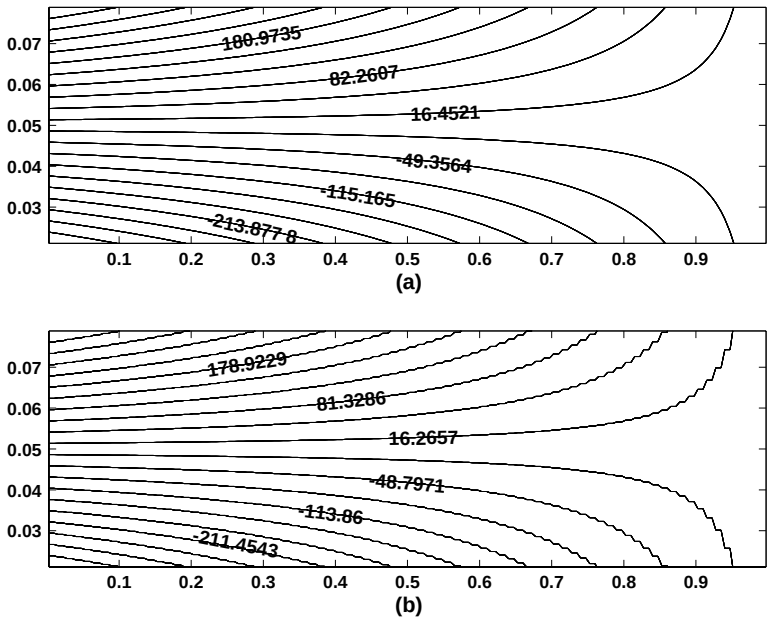

Fig. 6. Contour of stress σ_{xx} in N/m^2: $N = 1$. (a) Exact stress and (b) computed stress.

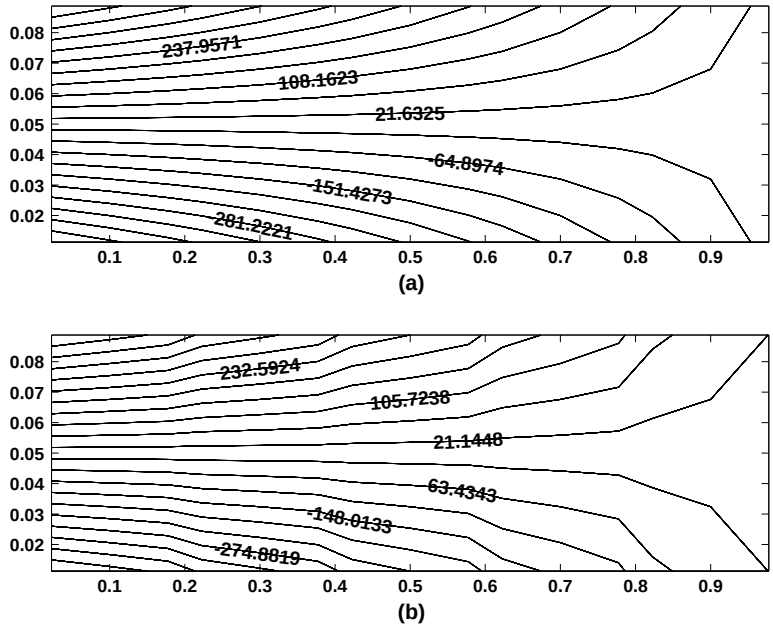

Fig. 7. Contour of stress σ_{xx} in N/m^2: $N = 2$. (a) Exact stress and (b) computed stress.

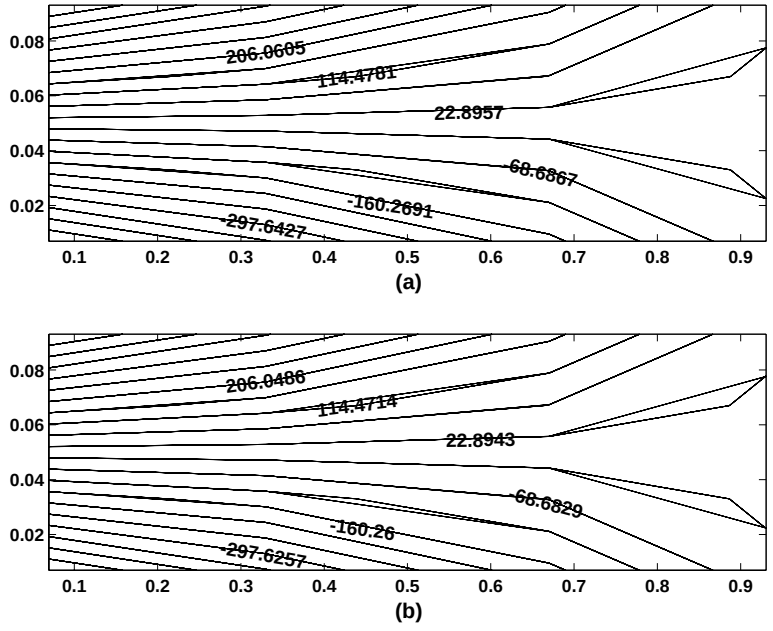

Fig. 8. Contour of stress σ_{xx} in N/m^2: $N = 3$. (a) Exact stress and (b) computed stress.

3.6. Summary of static analysis

The static analysis carried out in this section strongly supports the case in favour of CPE. The use of $N = 3$ elements is found to be very advantageous over lower order elements, in terms of accuracy as well as computational efficiency. Though the above study has been confined to isotropic case, the element is expected to give

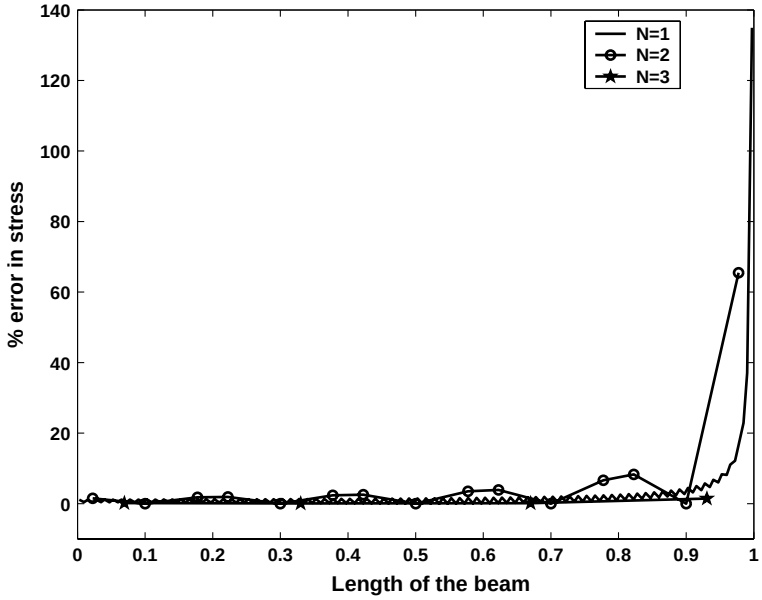

Fig. 9. Comparison of error in stress computation using $N = 1$, $N = 2$ and $N = 3$.

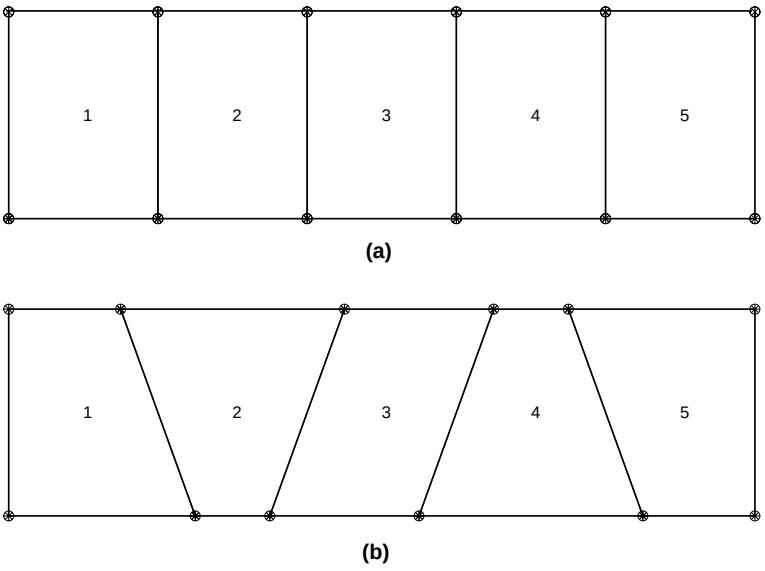

Fig. 10. (a) Undistorted mesh and (b) distorted mesh.

similar results for anisotropic and inhomogeneous materials as well, on account of the generality in formulation. The static analysis partially validates CPE thus enabling its use for dynamic analysis.

4. Analysis of free vibration problems

In this section, the predictive capability of the CPE is tested for free vibration problems. The elements are used to determine the natural frequencies for simple structures, where the analysis is carried out for both composite and FGM beams.

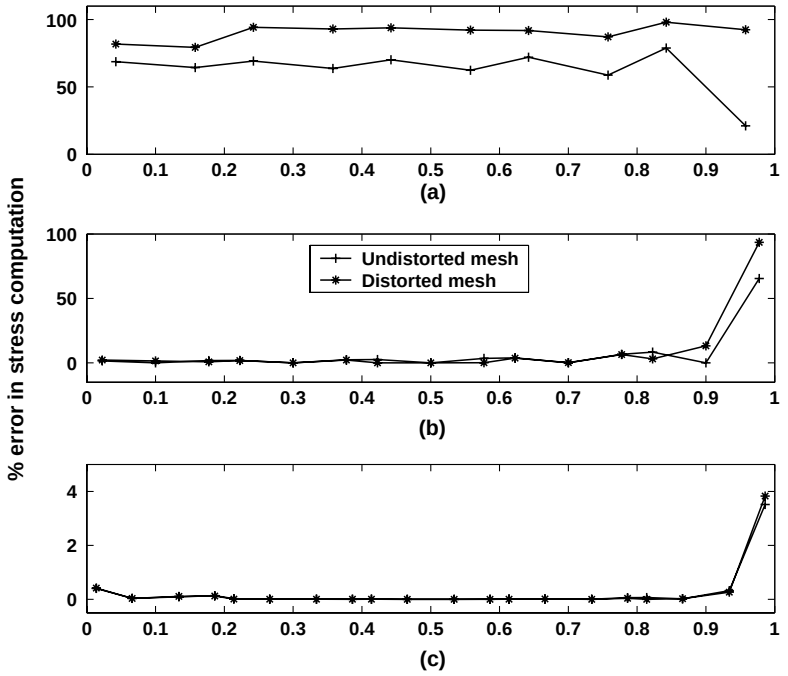

Fig. 11. Comparison of percentage error in stress (σ_{xx}) computation along the length of beam using undistorted and distorted meshes: (a) $N = 1$; (b) $N = 2$; (c) $N = 3$.

4.1. Anisotropic beam

A cantilever composite beam of span 1 m, depth 0.1 m and unit width is considered. The beam is made of GFRP, whose properties are $E_1 = 144.5$ GPa, $E_2 = 9.632$ GPa, $v_{12} = 0.3$, $v_{21} = 0.02$, $G_{12} = 4.128$ GPa and $\rho = 1389$ kg/m^3. All the fibers are assumed to be oriented along the axis of the beam.

The beam structure is subjected to free vibration analysis using the conventional FE as well as CPE. The number of elements required in each case to capture the first five natural frequencies with reasonable accuracy is given in Table V. The converged values of the first five natural frequencies of the beam obtained from each of the analysis is presented in Table VI. A comparison of the total memory used and CPU time taken for the above analysis is shown in Fig. 12.

Table V
Minimum number of elements required for free vibration analysis of composite beam

Number of elements	Lengthwise	Depthwise	Total
$N = 1$	75	10	750
$N = 2$	20	3	60
$N = 3$	3	1	3

Table VI
Converged values of first five natural frequencies of composite beam in rad/s for different values of N

	$N = 1$	$N = 2$	$N = 3$
ω_1	959.98	959.38	959.42
ω_2	4467.10	4460.50	4456.50
ω_3	9779.40	9761.10	9747.80
ω_4	15256.00	15222.00	15191.00
ω_5	16022.00	16022.00	16023.00

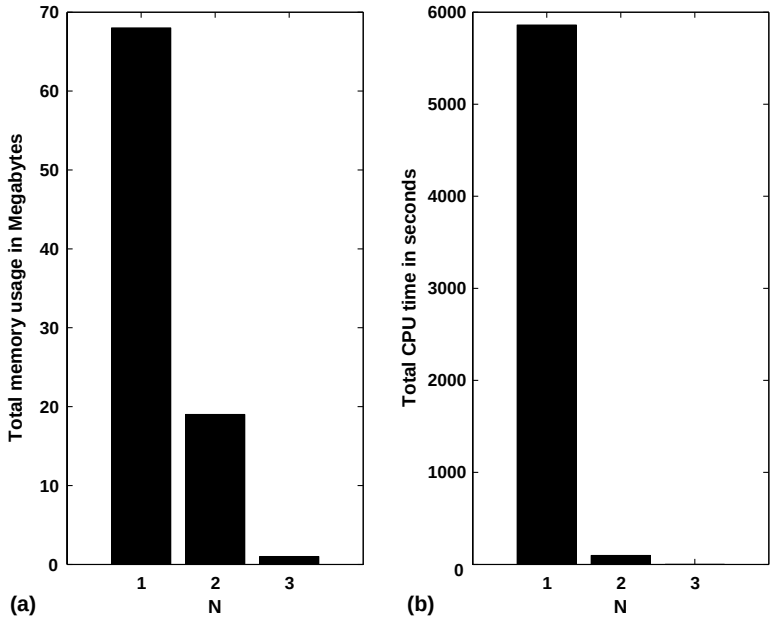

Fig. 12. Comparison of $N = 1$, $N = 2$ and $N = 3$ free vibration analysis of composite beam: (a) total Memory usage; (b) total CPU time.

As the bar plot suggests, the use of CPE has reduced the memory usage from 70 Mb to just 1 Mb. The computation time which is about 5860 s for FE i.e., $N = 1$, is as less as fraction of a second (0.2 s) for $N = 3$ CPE.

4.2. Inhomogeneous beam

The CPE is now tested for the analysis of a lengthwise graded FGM structure. A similar beam as the one used in the study of the variation of α and β is considered. The beam consists of a FGM sandwiched between steel and ceramic, whose material properties are as taken before. The variation of these properties is assumed to be exponential in the present case.

As in the case of composite beam, free vibration analysis is carried out to determine the first five natural frequencies of FGM beam. The number of elements required for each case of analysis is tabulated in Table VII. As is evident from the table, the number of CPE required is far less than the number of FE. It may be observed that just 8 CPE are sufficient to model the lengthwise gradation of properties of FGM as against the 100 and 25 elements required by $N = 1$ FE and $N = 2$ FE, respectively. The converged values of the first five natural frequencies of the beam obtained from each of the analysis is presented in Table VIII. A comparison of memory used and CPU time taken for each of these analysis is shown in Fig. 13.

As the figure suggests, the memory usage is reduced from about 117 Mb for FE ($N = 1$) to just 1 Mb for CPE. There is an enormous amount of reduction in CPU time as well. The analysis that requires a CPU time of about 17,000 s for $N = 1$ and 300 s for $N = 2$ analysis is completed in less than 6 s by CPE ($N = 3$).

The main reason for the drastic reduction in memory usage and CPU time for both composite as well as FGM is the use of just one element along the depth in the case of CPE. Conventional FE require discretization

Table VII
Minimum number of elements required for free vibration analysis of FGM beam

Number of elements	Lengthwise	Depthwise	Total
$N = 1$	100	10	1000
$N = 2$	25	3	75
$N = 3$	8	1	8

Table VIII
Converged values of first five natural frequencies of FGM beam in rad/s for different values of N

	$N=1$	$N=2$	$N=3$
ω_1	711.98	710.17	709.67
ω_2	4176.20	4165.40	4163.00
ω_3	10751.00	10752.00	10751.00
ω_4	11153.00	11121.00	11130.00
ω_5	20540.00	20457.00	20412.00

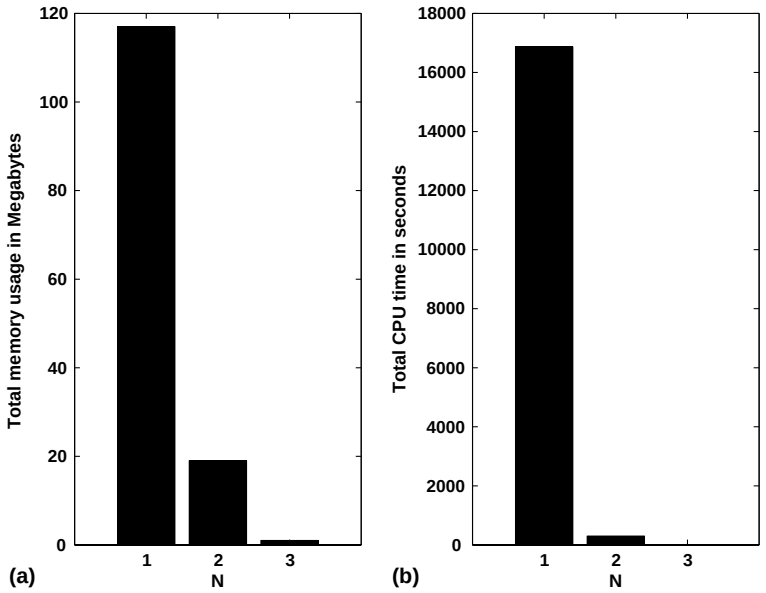

Fig. 13. Comparison of $N=1$, $N=2$ and $N=3$ free vibration analysis of FGM beam: (a) total Memory usage; (b) total CPU time.

of the structure along its depth as well. This leads to a larger bandwidth of the stiffness matrix resulting in need for large computational resources.

The analysis carried out in this section extends the use of CPE in two directions. Firstly, CPE has been successfully used for analysis of anisotropic and inhomogeneous materials. Secondly, the element has been subjected to dynamic analysis, the results for which are much better than the static analysis results.

5. Wave propagation analysis

The results in the previous two sections have indicated that CPE can be used very efficiently for accurately capturing higher order modes with least effort. These are fundamental to wave propagation problems in anisotropic and inhomogeneous media. In this section, wave propagation analysis is carried out on a variety of structures involving both composites and FGM. Initially analysis is carried out using a broadband pulse as the loading function. Later, a high frequency modulated pulse is allowed to propagate in a doubly bounded medium and its response is captured using CPE.

All the wave propagation simulations are compared with standard FE analysis with constant strain triangles (CST) mesh. This mesh is generated in a block of 4 elements and the inputs from the user are the number of blocks in the x- and y-directions. Thus, $6\times600\times4$ CST means there are 6 blocks depthwise, 600 blocks lengthwise and total $6\times600\times4=14{,}400$ elements are used.

Further, since most of the problems considered here involve smooth functions, the highest order of the polynomial in the examples is $N=3$. However, for the case of beam with horizontal crack higher order polynomials are also considered.

For time integration, the Newmark scheme is used with integration parameters $\alpha = 1/2$ and $\beta = 1/4$, which gives unconditionally stable scheme. For spatial discretization different grid points per wavelength (n_g) are used for different problems. For example, for anisotropic beam subjected to transverse load (1.0 m length), for $N = 1$, $n_g = 27$, for $N = 2$, $n_g = 11$ and for $N = 3$, $n_g = 7$. For $N = 3$ no appreciable dispersion is noticed even for this low value of n_g. This can be attributed to the consistent mass matrix formulation and the higher order of interpolation.

5.1. Response to broadband pulse

In this section, the response of structures to a time dependent load, which is in the form of a broadband pulse is studied. Analysis is carried out using a variety of structures like a simple beam, layer element etc. Both composites and FGM are considered for analysis. The loading function, as mentioned above, is in the form of a broadband pulse as shown in Fig. 14. As the figures shows, the load has a small duration of 50 μs and a frequency band of around 46 kHz, which excites numerous higher modes.

5.1.1. Anisotropic beam

A cantilever composite beam of span 1 m and depth 0.01 m is considered. The beam is made of GFRP, where all the layers are assumed to be oriented along the axis of the beam. The elastic properties are same as mentioned in previous example.

The composite beam is now subjected to a concentrated transverse load at the free end of the beam where The transverse velocity is also measured. The response obtained from analysis by FE and CPE is plotted in Fig. 15.

The number of elements required in each of the analysis is tabulated in Table IX. Fig. 16 gives a comparison of the memory used for stiffness matrix generation and the total CPU time taken for above analysis by $N = 1$, $N = 2$ and $N = 3$ elements.

As can be seen from Fig. 16, a lot of memory as well as computation time is saved by the use of CPE. The use of CPE has reduced the memory usage and CPU time by more that 50% of those required for lower order FE. The reason for this is that fewer elements are used along the depth when compared to FE.

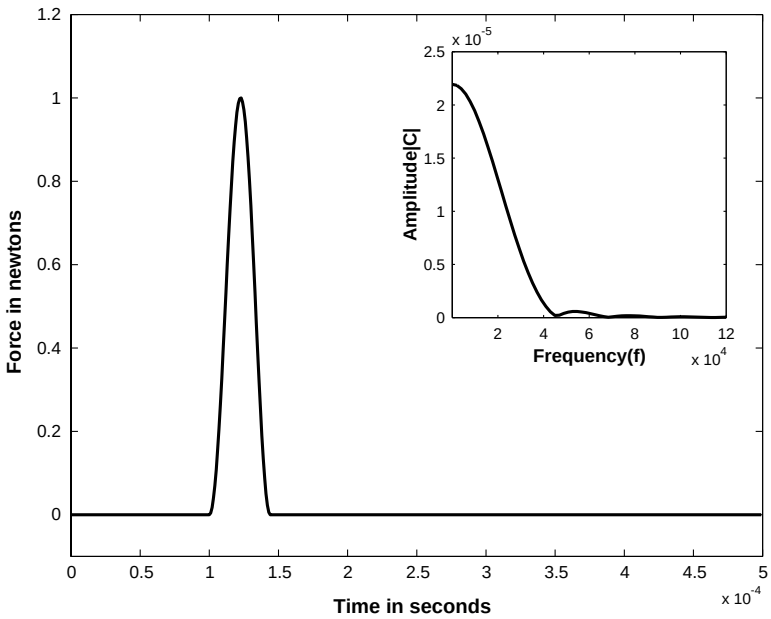

Fig. 14. Broadband pulse used for wave propagation analysis.

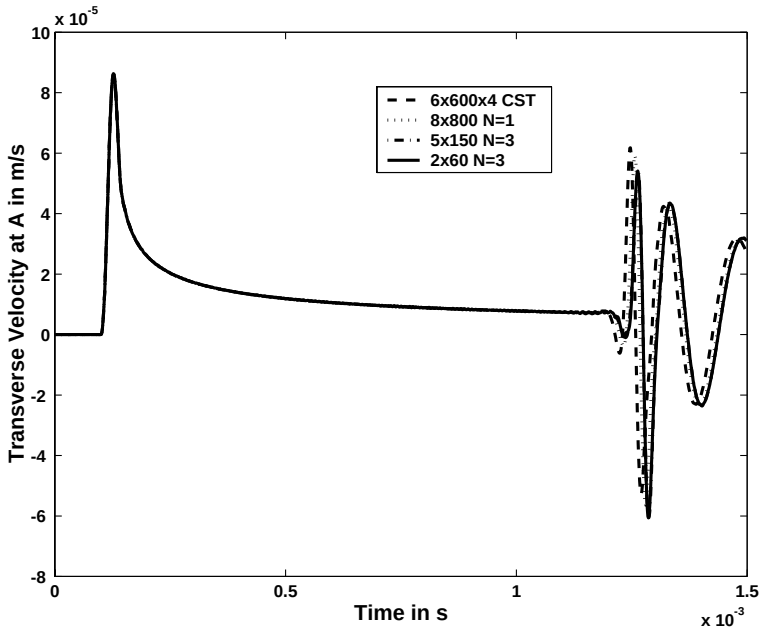

Fig. 15. Transverse response of composite beam to broadband pulse.

Table IX
Minimum number of elements required to capture transverse response of composite beam due to a broadband pulse

Element type	Number of elements		
	Lengthwise	Depthwise	Total
CST (modules)	600	6	14,400
$N = 1$	800	8	6400
$N = 2$	150	5	750
$N = 3$	60	2	120

5.1.2. Inhomogeneous beam

The above analysis is now carried out to the same inhomogeneous beam of previous examples, where it is subjected to a concentrated load at the free end transverse direction. The transverse velocity at the impact point is measured using FE and CPE. A comparison of the response is given in Fig. 17. The number of elements required to arrive at the converged response in each of the analysis is tabulated in Table X. Fig. 18 gives a comparison of the memory used for stiffness matrix generation and CPU time taken for each case of analysis. Both the memory as well as CPU time required for CPE are about one-third of those for $N = 1$ and about half of those for $N = 2$ analysis.

5.1.3. Anisotropic layer

In this section, the CPE is tested on a composite layer structure of length 1.0 m and depth 0.3 m consisting of three different ply-stackings (Fig. 19). The material is GFRP, with properties as taken previously. While the fibers of the top and bottom layers are oriented at 0°, the middle layer fibers are oriented at 90°.

The width of the structure is assumed to be 1 m for analysis. The bottom layer is fixed as shown. The structure is subjected to a concentrated load of unit magnitude at the point A shown in Fig. 19 in the transverse direction. The load is in the form of the broadband pulse (Fig. 14).

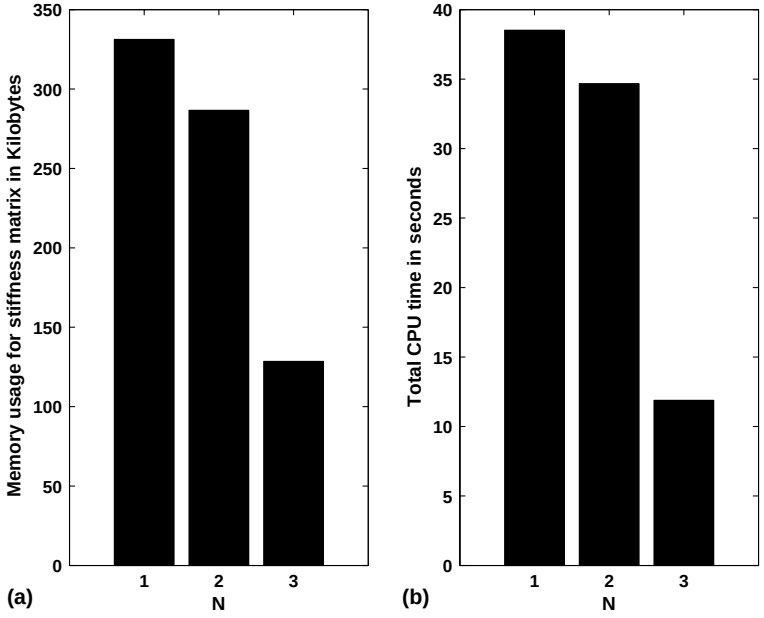

Fig. 16. Comparison of $N = 1$, $N = 2$ and $N = 3$ analysis for transverse response of composite beam to broadband pulse: (a) memory used for stiffness matrix; (b) total CPU time.

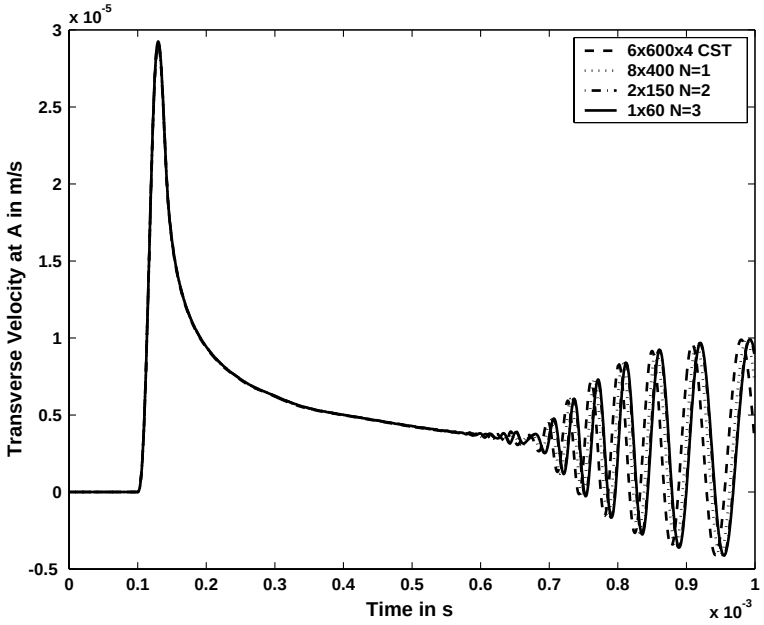

Fig. 17. Transverse response of FGM beam to broadband pulse.

Analysis is carried out using the FE and CPE. The transverse velocities at points A, B and C are measured. The responses obtained in the analysis are shown in Figs. 20–22, respectively. The number of elements used in each case for the above analysis is listed in Table XI.

It can be seen that the response obtained from constant strain triangle and $N = 1$ elements does not match with $N = 2$ and $N = 3$ responses. The reason for this is that a converged solution could not be obtained using the CST and $N = 1$ elements. In other words, CST and $N = 1$ elements require still more number of elements

Table X
Minimum number of elements required to capture transverse response of FGM beam due to a broadband pulse

Element type	Number of elements		
	Lengthwise	Depthwise	Total
CST (modules)	600	6	14,400
$N = 1$	800	4	3200
$N = 2$	150	2	300
$N = 3$	60	1	60

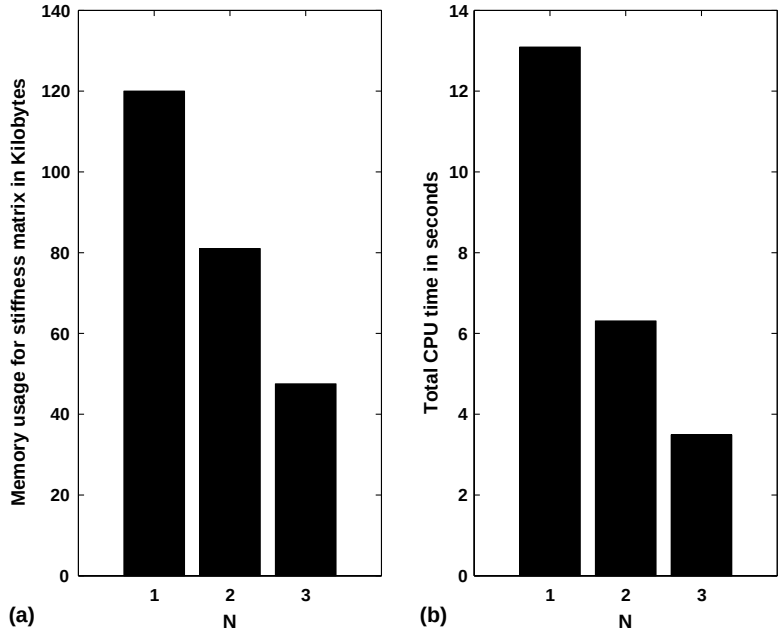

Fig. 18. Comparison of $N = 1$, $N = 2$ and $N = 3$ analysis for transverse response of FGM beam to broadband pulse: (a) memory used for stiffness matrix; (b) total CPU time.

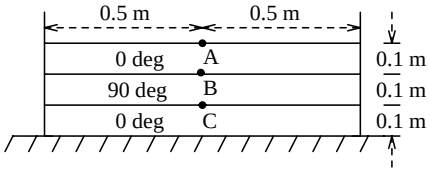

Fig. 19. Composite layer used for wave propagation analysis.

to get the required convergence. Fig. 23 gives a comparison of the memory usage and CPU time involved in $N = 2$ and $N = 3$ analysis. The advantage of using CPE is obvious from the comparison. The memory requirement as well as the analysis time have been almost halved when compared to those of FE ($N = 2$).

5.1.4. Inhomogeneous layer

Section 5.1.2 dealt with the analysis of a functionally graded beam with lengthwise gradation of properties. This section deals with the analysis of a FGM structure with depthwise gradation. The structure under consideration is of length 1.0 m and total depth of 0.5 m. The top and bottom 0.1 m of the layer structure consist

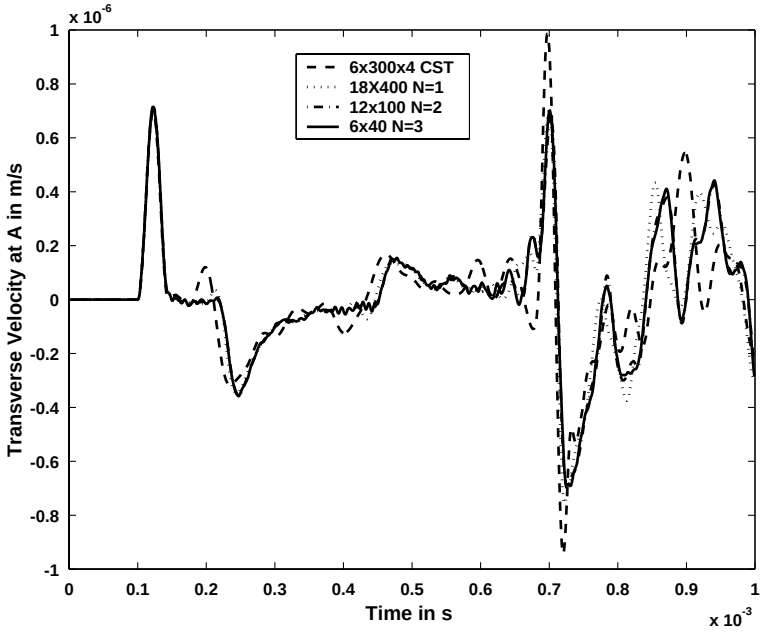

Fig. 20. Transverse response of composite layer at A due to broadband pulse.

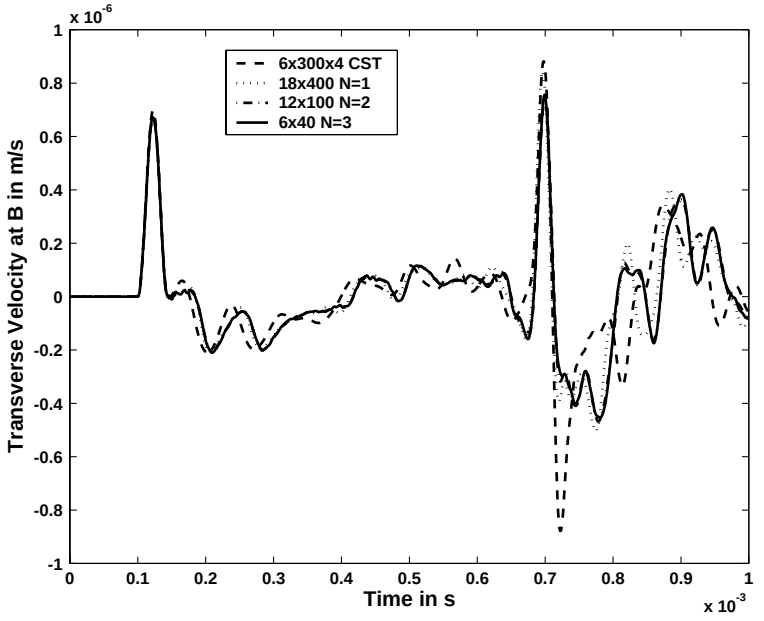

Fig. 21. Transverse response of composite layer at B due to broadband pulse.

of ceramic and steel, respectively. Between these layers is sandwiched a FGM layer of thickness 0.3 m as shown in Fig. 24.

The properties of steel and ceramic are taken the same as those considered previously. Unit width of the structure is considered for analysis. The FGM layer is subjected to a unit load at point A shown in Fig. 24 in the transverse direction in the form of broadband pulse. The responses are measured in terms of transverse velocities at the point of load application and at the interface between ceramic and FGM and between FGM

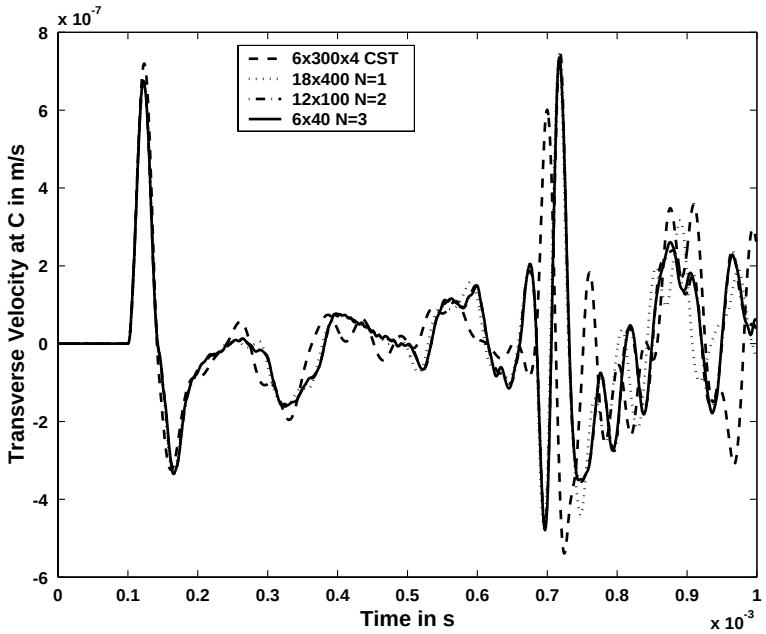

Fig. 22. Transverse response of composite layer at C due to broadband pulse.

Table XI
Minimum number of elements required to capture transverse response of composite layer structure due to a broadband pulse

Element type	Number of elements		
	Lengthwise	Depthwise	Total
CST (modules)	300	6	7200
$N = 1$	400	18	7200
$N = 2$	100	12	1200
$N = 3$	40	6	240

and steel i.e., at points A, B and C shown. The respective responses are as shown in Figs. 25–27. Also, the number of elements used in each case for the above analysis is tabulated in Table XII.

In this case also, the CST and $N = 1$ elements show little deviation from the converged solution. The reason for this is that a large number of lower order elements are required to model the depthwise gradation of properties with reasonable accuracy. The same has been modeled with just 20 for $N = 2$ elements and 10 for $N = 3$ elements along the depth. A comparison of the memory usage and analysis time for $N = 2$ and $N = 3$ elements is shown in Fig. 28. Fig. 28 suggests that there is almost 40–50% reduction in memory usage and CPU time for analysis by the use of CPE.

The superiority of the CPE is reflected in each of the above analysis. Problems which could not be solved accurately by FE have been solved with high accuracy and with reasonably low computational resources, thus encouraging the use of CPE for solving wave propagation problems involving longer propagation distances and high frequency loads.

5.2. Response to modulated pulse

In this section, the CPE is used to carry out analysis involving a high frequency load. The loading function is in the form of a modulated pulse with a central frequency of 80 kHz. The time and frequency domain

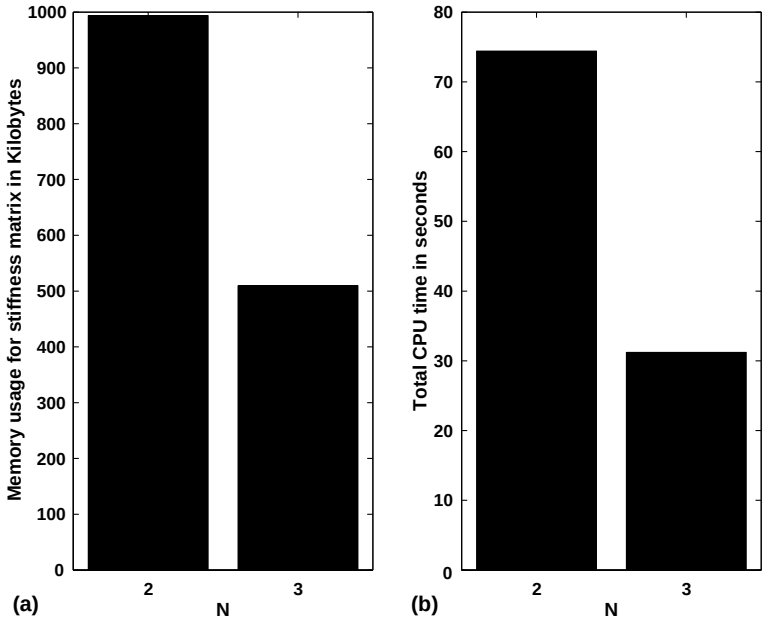

Fig. 23. Comparison of $N = 2$ and $N = 3$ analysis for transverse response of composite layer to broadband pulse: (a) memory used for stiffness matrix; (b) total CPU time.

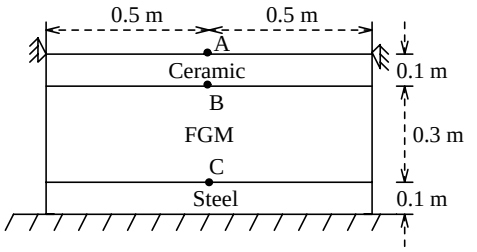

Fig. 24. Inhomogeneous layer used for wave propagation analysis.

response of the pulse is shown in Fig. 29. The modulated pulse is used to carry out analysis on composite beams as is done with the broadband pulse. The reason for using a modulated pulse is to capture the additional modes (Mahapatra et al., 2000) that propagate in asymmetric composite structures.

5.2.1. Anisotropic beam

5.2.1.1. Axial case. A cantilever composite beam of span 10.0 m, depth 0.001 m and unit width is considered for analysis, where the material is same as the one used previously. Two cases are considered, one a uniaxial composite with all the layers oriented along the length of the beam and secondly, a cross-ply beam with the bottom half layers at 0° and top half layers at 90°.

The beams are subjected to a distributed axial load of unit magnitude at the free end of the beam. The response is measured in terms of axial velocity at the topmost layer of the free end of the beam. Analysis is carried out using CPE ($N = 3$). The response obtained in each case is shown in Fig. 30. As can be seen from the response, for a uniaxial ply, the incident pulse and its reflection from the fixed end have been captured distinctly. The cross-ply response consists of an additional reflection. This corresponds to the flexural mode arising out of axial–flexural coupling in an asymmetric composite structure. The analysis has required the use of about 500 CPE.

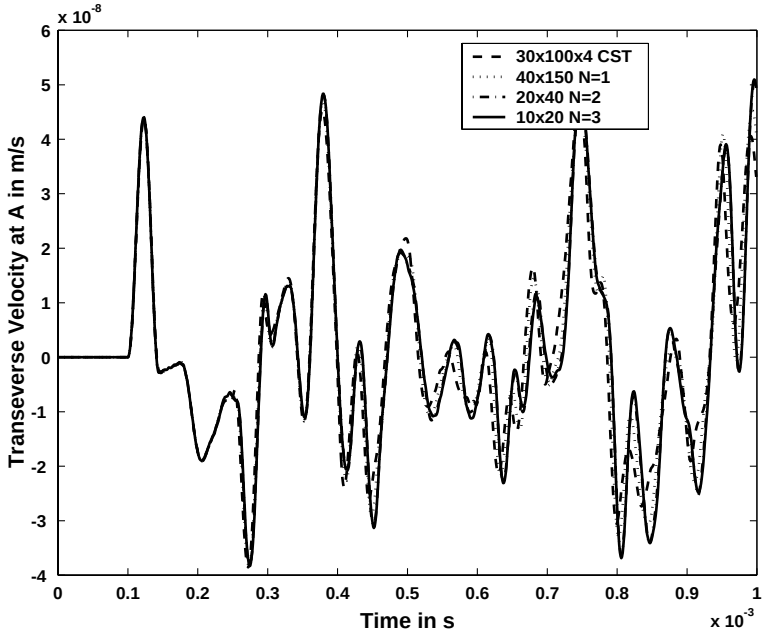

Fig. 25. Transverse response of depthwise FGM layer at A due to broadband pulse.

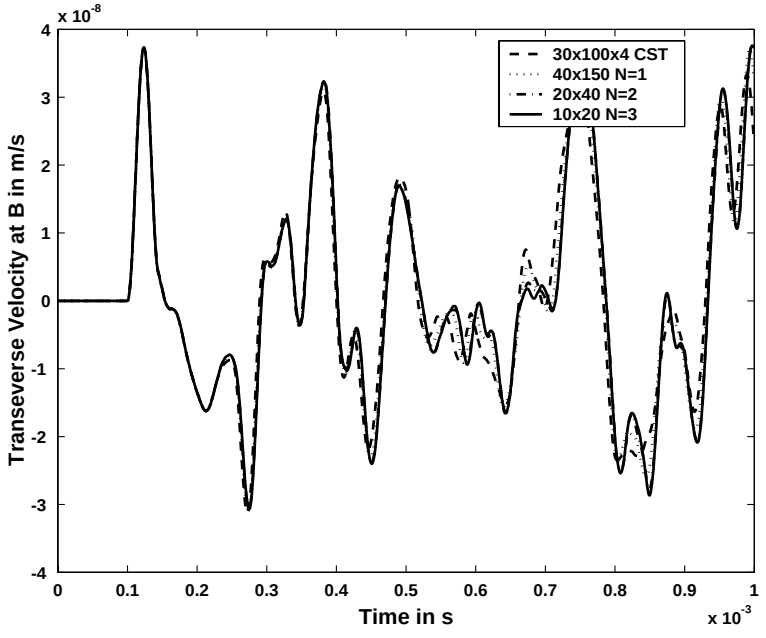

Fig. 26. Transverse response of depthwise FGM layer at B due to broadband pulse.

5.2.1.2. Transverse case. The same cantilever composite beams of previous example are considered, where the length is now changed to 1.5 m. The beam is subjected to a concentrated load of unit magnitude at the free end in the form of the modulated pulse. Using CPE, analysis is carried out to record the transverse velocity at the free end of the beam, which is shown in Fig. 31. For transverse analysis also, only the incident and reflected pulse are seen for a symmetric composite beam. On the other hand, the axial mode due to axial–flexural

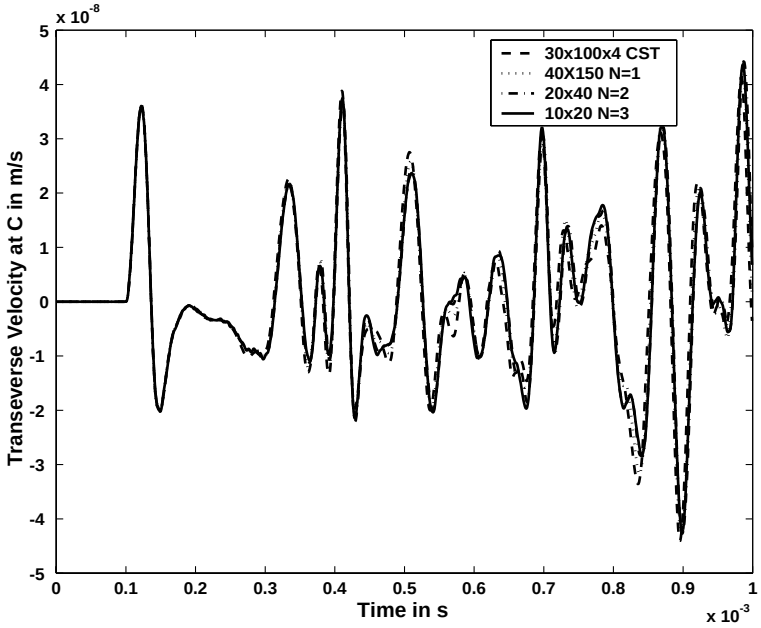

Fig. 27. Transverse response of depthwise FGM layer at C due to broadband pulse.

Table XII
Minimum number of elements required to capture transverse response of depthwise FGM layer structure due to a broadband pulse

Element type	Number of elements		
	Lengthwise	Depthwise	Total
CST (modules)	100	30	12,000
$N = 1$	150	60	6000
$N = 2$	40	20	800
$N = 3$	20	10	200

coupling (and its reflections) can be observed after the incident pulse for the asymmetric composite beam. About 500 CPE are required to obtain the above response accurately.

In the analysis involving modulated pulse, the propagating distance of the wave is reasonably long. The first reflection of the wave was captured after it traveled 20 m for axial case and 3 m for transverse case. From the results, one can infer that axial wave travels faster that transverse wave. Moreover, the velocity of wave is higher in symmetric composite than in asymmetric composite beam.

6. Wave propagation in cracked structures

This section attempts to use the CPE to carry out wave scattering studies on a cracked structure. Few cases are studied where crack is detected in a structure using broadband and modulated pulse.

6.1. Modeling of the crack

The following approach is adopted to model crack in a structure. Initially the structure is meshed without any attempt to model the crack. Then the nodes and elements that are affected by the crack are identified from the location and length of the crack. At the nodes that are affected by the crack, duplicate nodes are generated. Thus the total number of nodes in the structure increases by the number of nodes affected by the crack. Then the nodes in the mesh are renumbered in such a way as to keep the bandwidth minimum. While generating the

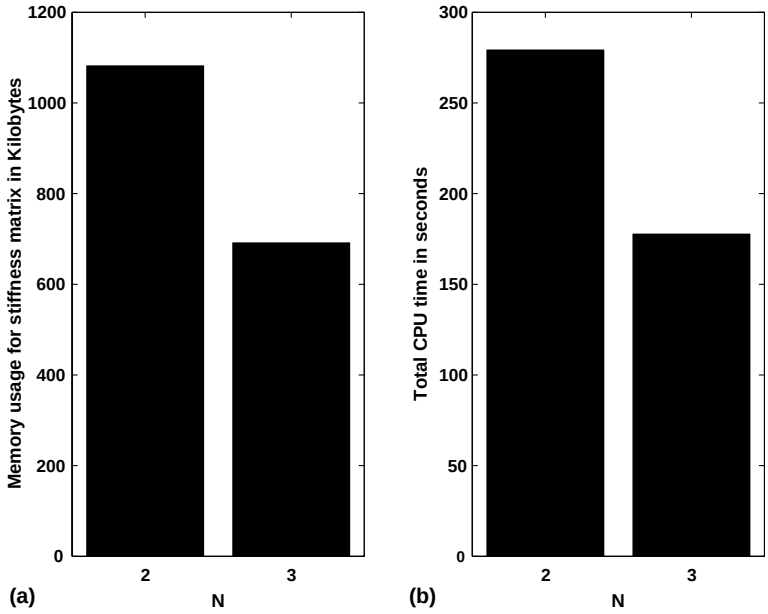

Fig. 28. Comparison of $N = 2$ and $N = 3$ analysis for transverse response of depthwise FGM layer to broadband pulse: (a) memory used for stiffness matrix; (b) total CPU time.

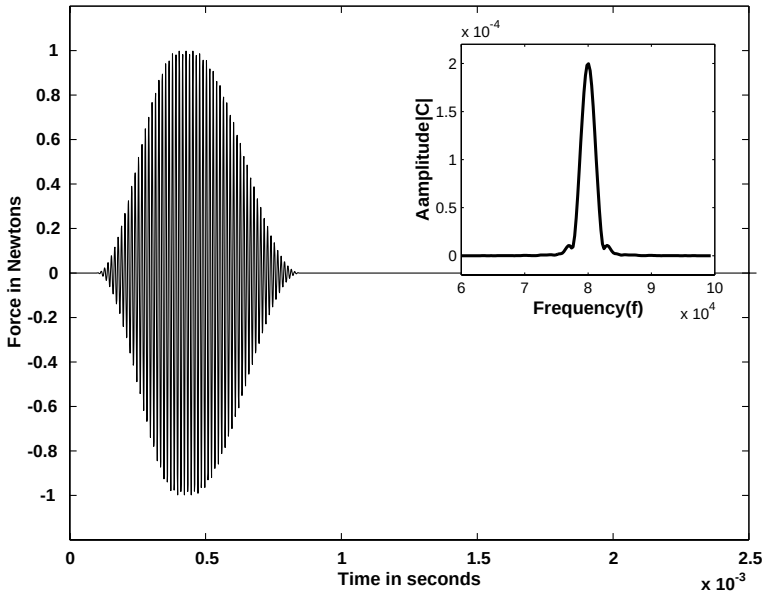

Fig. 29. Modulated pulse used for wave propagation analysis.

connectivity in each element, the original node number is used if the element is below or to the left of crack and duplicate node number is used if it is above or to the right of the crack.

In the present study, a simplified approach is adopted where the structure is considered to be rectangular and the crack is assumed to be oriented along one of its axes. The creation of duplicate nodes and renumbering is schematically explained for horizontal crack and vertical crack in Figs. 32 and 33, respectively.

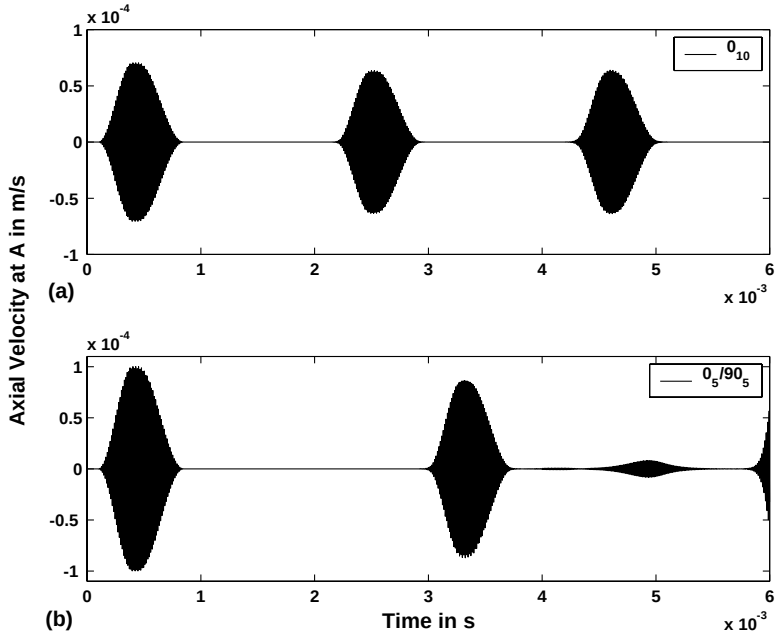

Fig. 30. Axial response of composite beam at A due to modulated pulse: (a) 0_{10}; (b) $0_5/90_5$.

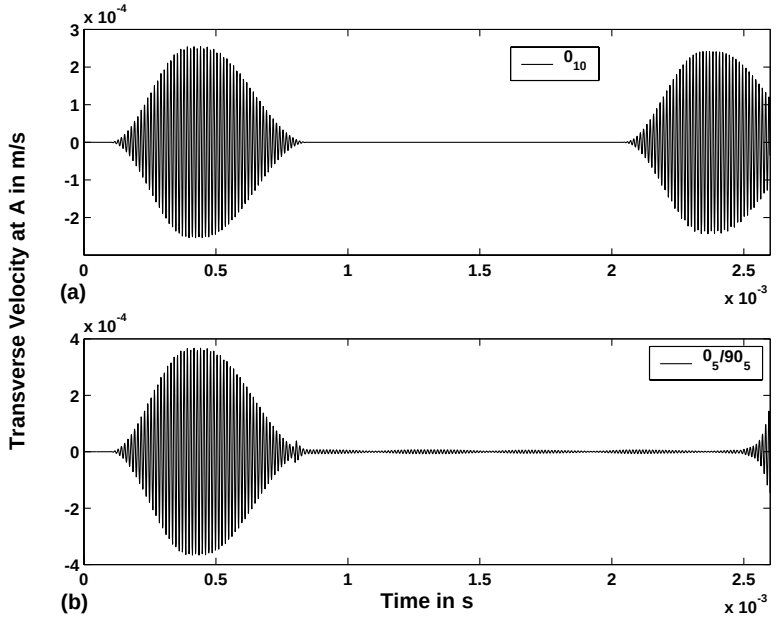

Fig. 31. Transverse response of composite beam at A due to modulated pulse: (a) 0_{10}; (b) $0_5/90_5$.

6.2. Anisotropic beam

The structure considered for crack detection is the same composite beam that was used to carry out transverse analysis using modulated pulse. Analysis is carried out for two cases, one with crack oriented in horizontal direction and the other with crack oriented in vertical direction. The structure without crack, with

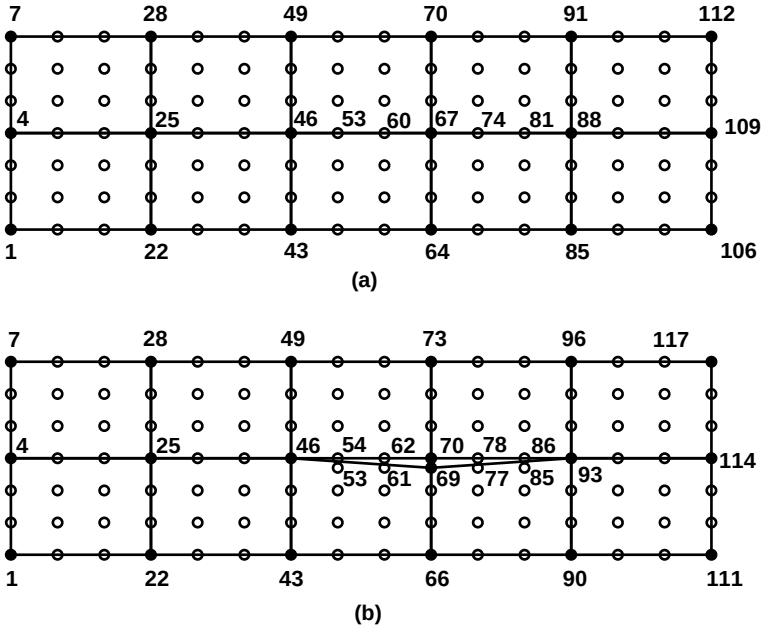

Fig. 32. Modelling of horizontal crack: (a) mesh without crack; (b) mesh with crack.

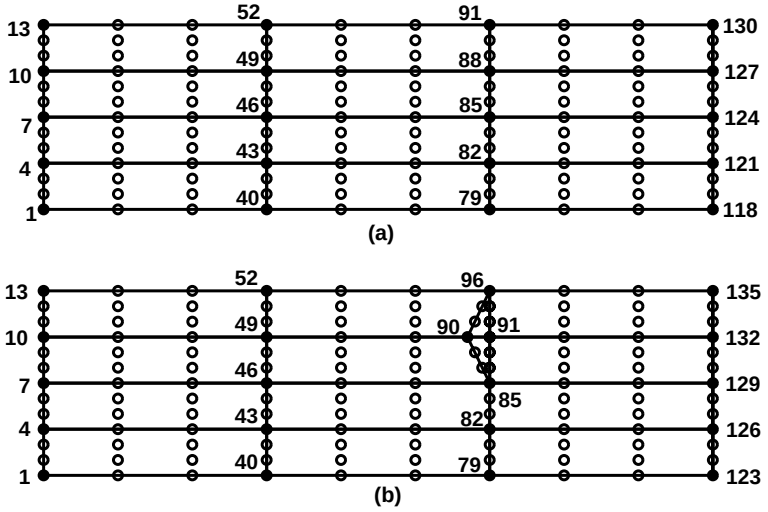

Fig. 33. Modelling of vertical crack: (a) mesh without crack (b) mesh with crack.

horizontal crack and with vertical crack are shown in Fig. 34. These structures are analyzed using broadband pulse and modulated pulse. The broadband pulse and modulated pulse are the same as ones used in previous example.

6.2.1. Horizontal crack

The beams shown in Fig. 34(a) and (b) are subjected to a unit concentrated load at the free end in transverse direction. The response is measured in terms of transverse velocity at point A. The response obtained in

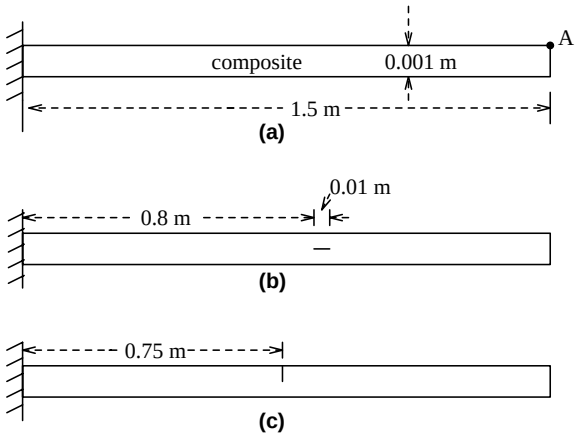

Fig. 34. Composite beam for used for crack detection: (a) beam without crack; (b) beam with horizontal crack; (c) beam with vertical crack.

uncracked and cracked structure for broadband pulse and 80 kHz modulated pulse are shown in Figs. 35 and 36, respectively.

In the analysis using broadband pulse, in cracked structure, scattering in the wave from the crack can be observed. One can clearly distinguish between the reflection of wave from crack and that from fixed end. Similarly, the use of modulated pulse leads to a clear and conclusive response. Only the original pulse and its reflection from the fixed end is observed in the uncracked structure, whereas, in the presence of a crack, the reflection of the modulated pulse can be distinctly observed between incident pulse and its reflection from fixed end.

To further explore the efficiency of the CPE, the same beam is considered with larger crack length (0.3 m). The crack is centrally placed in the structure at mid-depth. The order of the polynomial considered is $N = 1$–6.

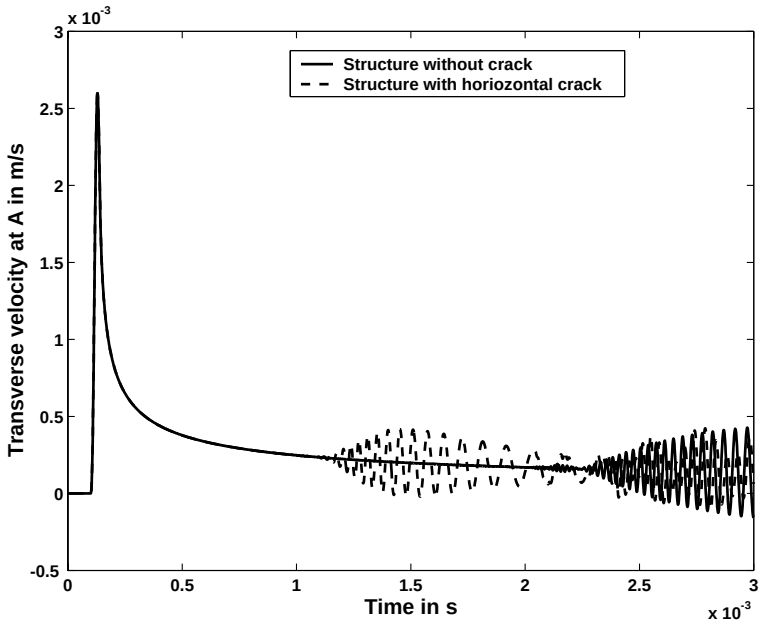

Fig. 35. Transverse response to broadband pulse of composite beam without crack and with horizontal crack.

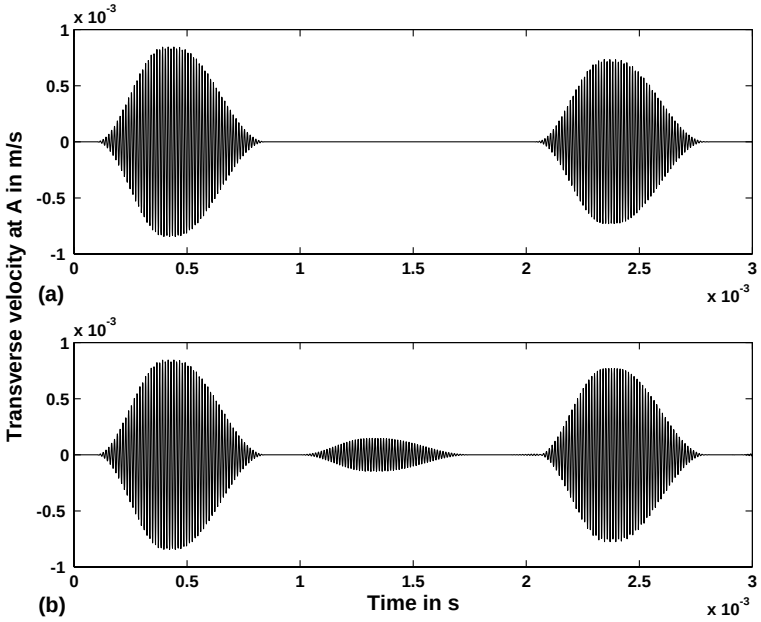

Fig. 36. Transverse response to modulated pulse of composite beam: (a) without crack; (b) with horizontal crack.

The minimum number of elements required in each case is given in Table XIII, which shows drastic reduction of the number of elements with increasing N.

6.2.2. Vertical crack

The beam shown in Fig. 34(c) has a vertical crack at its mid span length from the top edge to half its depth. This is now subjected to a transverse load of unit magnitude at the free end. The load is applied in the form of a broadband pulse and modulated pulse separately. The responses obtained in this case are compared with the respective responses obtained for uncracked structure (Fig. 34(a)). The response of the structure to broadband pulse is shown in Fig. 37 and to modulated pulse is shown in Fig. 38.

In Fig. 37 the scattering of the broadband pulse from crack is very less making it almost impossible to detect. However, the response from modulated pulse shown in Fig. 38 clearly suggests the presence of crack. The reflection from the crack can be seen distinctly between incident pulse and its reflection from fixed end of beam. The reason for this is the very minute size of the crack. The length of the crack is just 0.0005 m or 0.5 mm, which is half the depth of beam. The analysis shows the advantage of using a modulated pulse for detecting minute cracks and small discontinuities in structures. Another noteworthy point is that the above analysis has required the use of 2000 (500 lengthwise and 4 depthwise) CPE. In spite of the use of these many higher order elements, the analysis was completed in just 20 min with the use of 67 Mb memory. It can be said

Table XIII
Minimum number of elements required to capture scattering due to horizontal crack within acceptable accuracy

Polynomial order (N)	Number of elements			
	Lengthwise	Depthwise	Total	Along the crack
1	1200	2	2400	240
2	500	2	1000	100
3	150	2	300	30
4	100	2	200	20
5	75	2	150	15
6	50	2	100	10

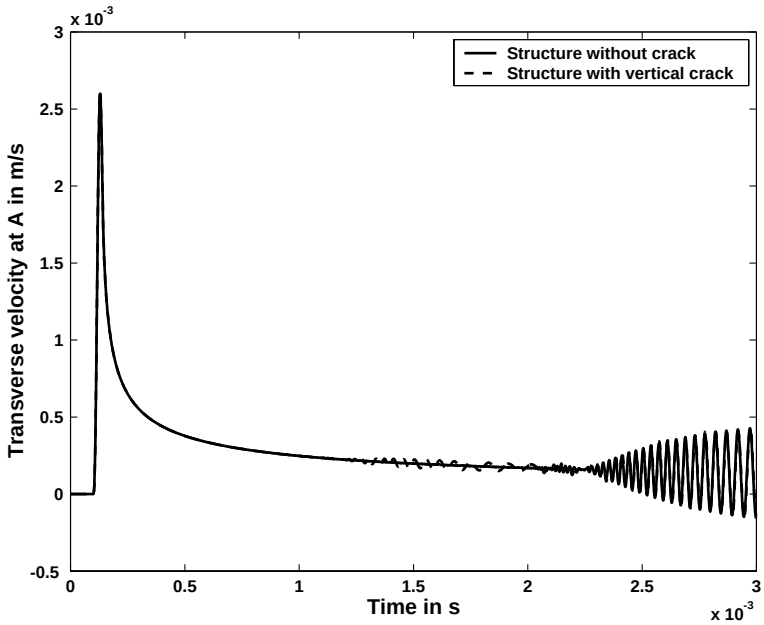

Fig. 37. Transverse response to broadband pulse of composite beam without crack and with vertical crack.

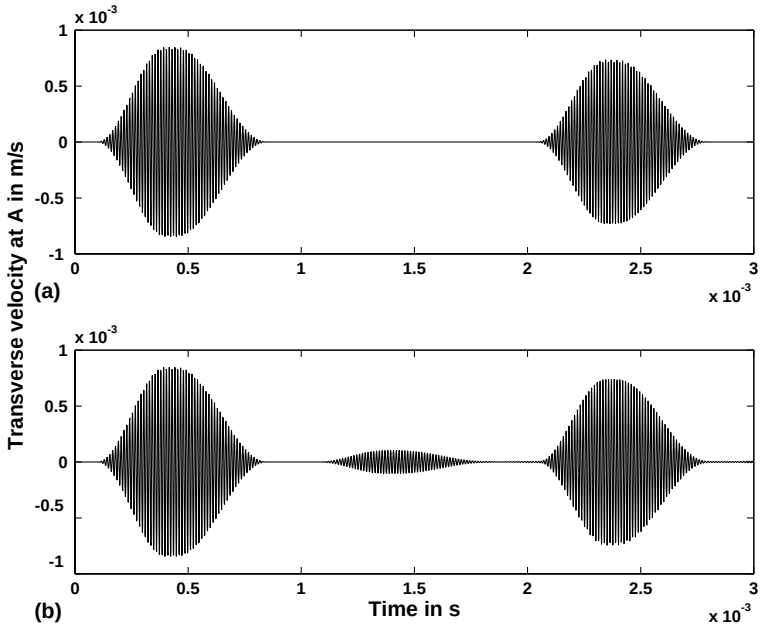

Fig. 38. Transverse response to modulated pulse of composite beam: (a) without crack; (b) with vertical crack.

that the above analysis would be very difficult to carry out accurately using conventional FE with limited computational resources. The reason for this is that it would require many elements depthwise to model the vertical crack in beam. This would amount to increasing the memory requirement enormously.

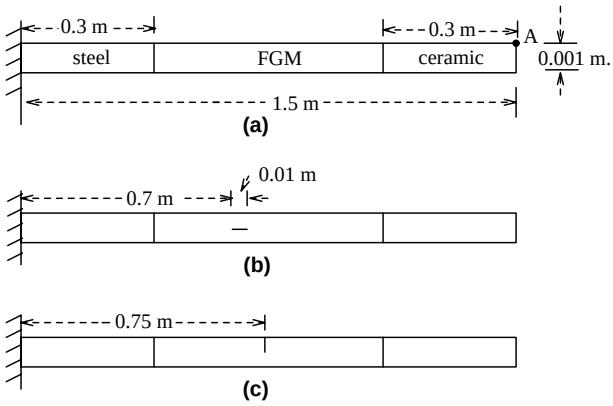

Fig. 39. FGM beam for used for crack detection: (a) beam without crack; (b) beam with horizontal crack; (c) beam with vertical crack.

6.3. Inhomogeneous beam

In this section CPE is used to detect cracks in a FGM beam. The beam under consideration is same as the one used to carry out wave propagation analysis using modulated pulse in the previous chapter. The beam consists of steel, FGM and ceramic sections over different lengths as shown in Fig. 39(a). Fig. 39(b) and (c) show the beam with horizontal crack and vertical crack, respectively.

6.3.1. Horizontal crack

The uncracked FGM beam and the FGM beam with horizontal crack are subjected to a concentrated unit transverse load at the free end in the form of broadband pulse and modulated pulse separately. In each case, the transverse velocity at point A shown in Fig. 39(a) is measured. The response obtained for broadband pulse and modulated pulse are given in Figs. 40 and 41, respectively.

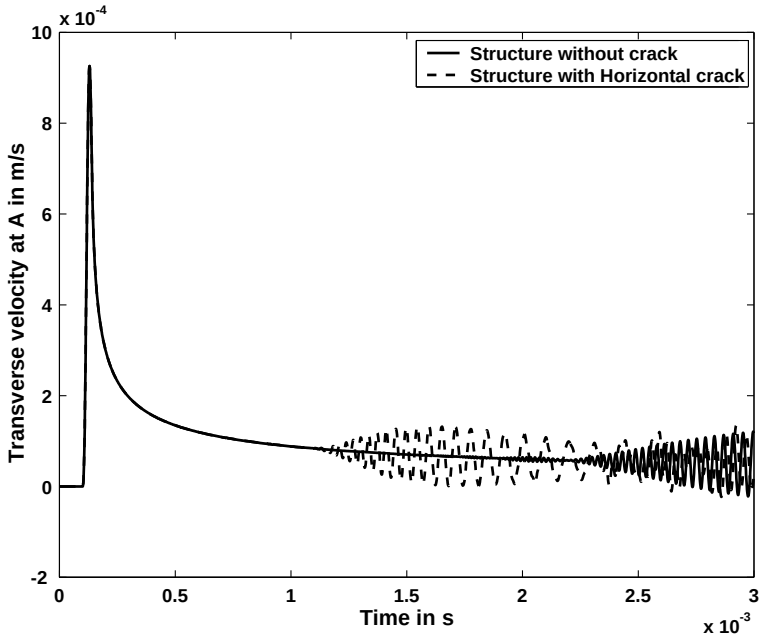

Fig. 40. Transverse response to broadband pulse of FGM beam without crack and with horizontal crack.

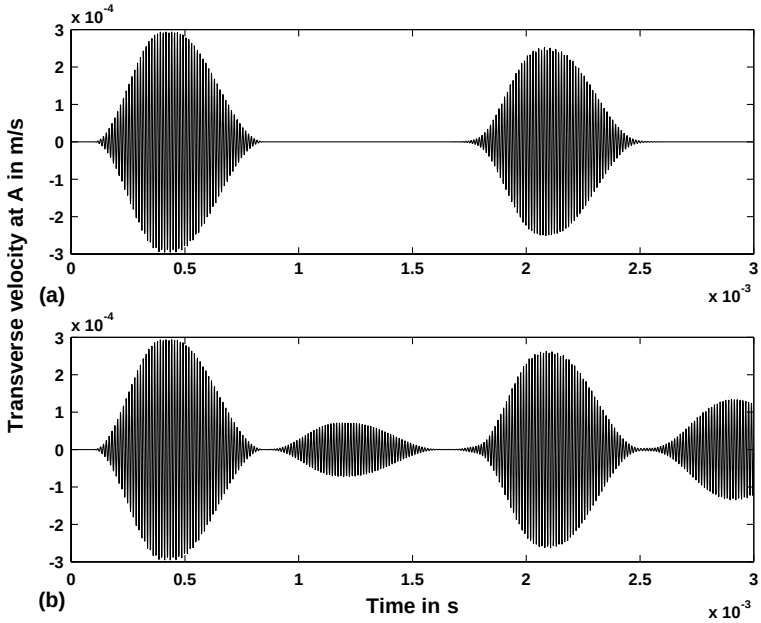

Fig. 41. Transverse response to modulated pulse of FGM beam: (a) without crack; (b) with horizontal crack.

The reflection of the pulse from the crack as well as the fixed end can be observed in each of the above responses. Once again, the reflection from crack is distinctly seen.

6.3.2. Vertical crack

The FGM beam with a vertical crack shown in Fig. 39(c) is subjected to transverse load in the form of broadband pulse and modulated pulse separately. The response in each case is measured in terms of the

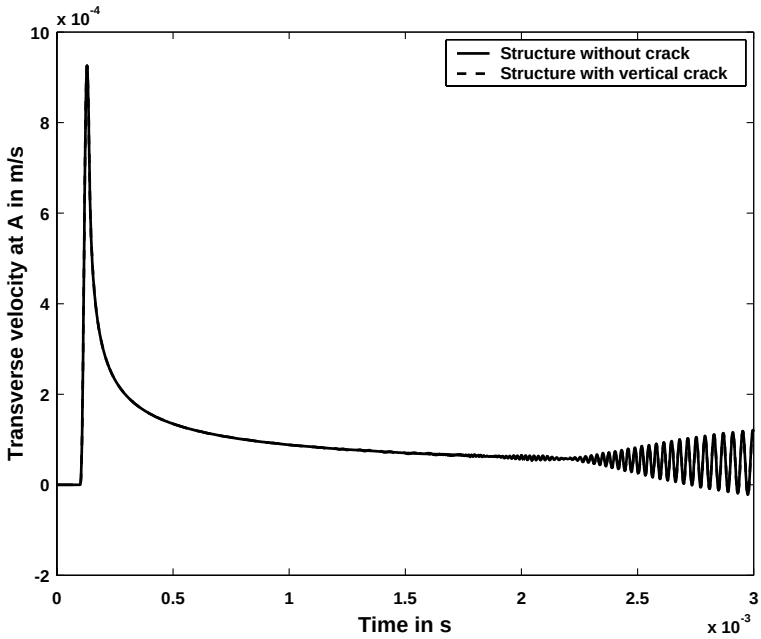

Fig. 42. Transverse response to broadband pulse of FGM beam without crack and with vertical crack.

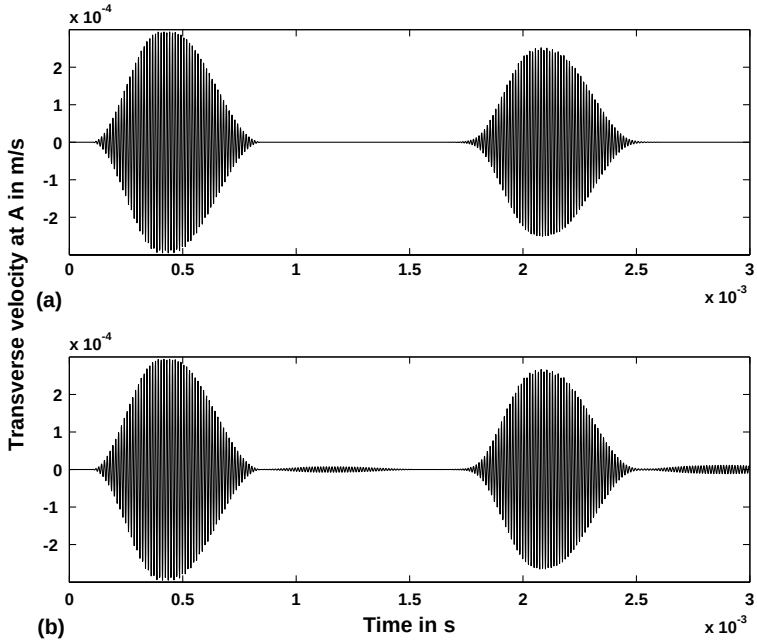

Fig. 43. Transverse response to modulated pulse of FGM beam: (a) without crack; (b) with vertical crack.

transverse velocity at point A. The responses obtained in each case are compared with those obtained for uncracked section shown in Fig. 39(a). The responses obtained for broadband pulse and modulated pulse are shown in Figs. 42 and 43, respectively.

The response to broadband pulse cannot detect the presence of the crack. On the other hand, in the analysis using modulated pulse the crack is detected in the from of small scattering. Thus, modulated pulse is more effective in detecting crack than broadband pulse. The above analysis required as many as 2400 elements (600 lengthwise and 4 depthwise). The analysis was complete in about 20 min and required 79 Mb of memory. To model the lengthwise FGM as well as depthwise crack using lower order FE will require a large number of elements. Further, capturing such small reflections from crack tip may require even further refinement of the mesh, thus making the process cumbersome and time consuming.

7. Conclusion

The use of CPEM for wave propagation analysis of anisotropic and inhomogeneous structures is successfully demonstrated. The method is highly successful in overcoming the shortcomings of FE. Problems which could not be tackled by FE due to requirement of a very fine mesh and hence a large number of elements, enormous memory and computation time, are handled by CPE with ease.

As the formulation is similar to FE, the implementation is very simple. The static analysis which involved isotropic beam showed that CPE could produce accurate results using fewer elements than FE. The prediction of stresses are highly accurate. The error in stress computation is minimal when compared to the stresses obtained from lower order FE. Moreover, error in stress computation induced by mesh distortion is negligible for CPE. Further, static problems of beams having very high span to depth ratio are solved effortlessly. On the other hand, conventional FE fails after a certain limit. The free vibration analysis demonstrates the spectral convergence of CPE. Analysis which took over a couple of hours to solve by FE are completed in about one-tenth of a second. Time apart, a lot of memory has also been saved by the use of CPE.

CPE is found to be at ease in handling wave propagation problems in anisotropic and inhomogeneous media. The reduction in computation time and memory usage especially for layer structures are appreciably high. Wave propagation analysis in thin doubly bounded media over long propagating distances using high frequency modulated pulse are carried out. Lastly, the CPE has been successfully used for crack detection

problems. Problems involving detection of cracks oriented horizontally and vertically in composite and FGM beams are solved. Cracks as small as 0.0005 m or 0.5 mm could be detected using a high frequency modulated pulse. The effectiveness of using modulated pulse for crack detection and its advantage over broadband pulse is demonstrated.

In summary, a numerical tool is developed and tested in the form of Chebyshev pseudospectral finite element method, to carry out wave propagation analysis of anisotropic and inhomogeneous materials. The tool is highly successful in two ways. Firstly, the computation cost (in terms of memory usage and CPU time) incurred in solving wave propagation problems by FE is reduced considerably. Second, complex problems involving complicated geometries and high frequency loads, which FE cannot handle can now be solved easily.

The present work can be stated to be of a very significant nature. This can be used as a launch-pad for extending CPE for various kinds of problems pertinent to the field of structural analysis.

References

Boyd, J.P., 2000. Chebyshev and Fourier Spectral Methods, second ed. Dover Publications Inc., New York.

Canuto, C., Hussaini, M.Y., Quarteroni, A., Zang, T.A., 1988. Spectral Methods in Fluid Dynamics. Springer-Verlag Series, Berlin.

Chakraborty, A., Gopalakrishnan, S., Reddy, J.N., 2003. A new beam finite element for the analysis of functionally graded materials. Int. J. Mech. Sci. 45 (3), 519–539.

Cook, R.D., Malkus, D.S., Plesha, M.E., 1989. Concepts and Applications of Finite Element Analysis, third ed. John Wiley & Sons, Singapore.

Dauksher, W., Emery, A.F., 1997. Accuracy in modelling the acoustic wave equation with chebyshev spectral finite elements. Finite Elem. Anal. Des. 26, 115–128.

Dauksher, W., Emery, A.F., 1999. An evaluation of the cost effectiveness of chebyshev spectral and *p*-finite element solutions to the scalar wave equation. Int. J. Numer. Methods Eng. 45, 1099–1113.

Dauksher, W., Emery, A.F., 2000. The solution of elastoplastic and elastodynamic problems with chebyshev spectral finite elements. Comput. Methods Appl. Mech. Eng. 188, 217–233.

Doyle, J.F., 1997. Wave Propagation in Structures, second ed. Springer-Verlag Series, Berlin.

Gottlieb, D., Orzag, S.A., 1977. Numerical analysis of spectral methods: theory and application. In: Regional Conference Series in Applied Mathematics. SIAM, Philadelphia.

Gupta, U.S., Lal, R., 1985. Axisymmetric vibrations of polar orthotropic Mindlin annular plates of variable thickness. J. Sound Vib. 98, 565–573.

Jackiewicz, Z., Renaut, R.A., 2002. A note on stability of pseudospectral methods for wave propagation. J. Comput. Appl. Math. 143, 127–139.

Lee, J., 1998. Application of pseudospectral method to the analysis of Reissner–Mindlin plates. J. Kor. Soc. Mech. Eng. 22, 2136–2145.

Lee, J., Schultz, W.W., 2004. Eigen value analysis of Timoshenko beams and axisymmetric Mindlin plates by the pseudospectral method. J. Sound Vib. 269, 609–621.

Mahapatra, D.R., Gopalakrishnan, S., Sankar, T.S., 2000. Spectral element based solutions for wave propagation analysis of multiply connected unsymmetric laminated composite beams. J. Sound Vib. 237 (5), 819–836.

Padovani, E., Priolo, E., Seriani, G., 1994. Low- and high-order finite element method: experience in seismic modeling. J. Comput. Acoustics 2, 371–422.

Patera, A.T., 1984. A spectral element method for fluid dynamics: laminar flow in channel expansion. J. Comput. Phys. 54, 468–488.

Priolo, E., Carcione, J., Seriani, G., 1994. Numerical simulation of interface waves by high-order spectral modeling techniques. J. Acoust. Soc. Am. 95, 681–693.

Reddy, J.N., 1997. Mechanics of Laminated Composite Plates: Theory and Analysis. CRC, Boca Raton, FL.

Seriani, G., 2004. Double-grid chebyshev spectral elements for acoustic wave modeling. Wave Motion 39, 351–360.

Seriani, G., Priolo, E., 1994. Spectral element method for acoustic wave simulation in heterogeneous media. Finite Elem. Anal. Des. 16, 337–348.

Soni, S.R., Amba-Rao, C.L., 1975. On radially symmetric vibrations of orthotropic non-uniform disks including shear deformation. J. Sound Vib. 42, 57–63.